EUROPEAN ORGANIZATION FOR NUCLEAR RESEARCH

CERN BIBLIOTHEQUE
SCP
CERN SPSC
88-22

CERN LIBRARIES, GENEVA
SC00000535

CERN/SPSC 88–22
SPSC/P 236
June 15, 1988

ADDENDUM TO MEMORANDUM M 406

STUDY OF RELATIVISTIC NUCLEUS–NUCLEUS COLLISIONS AT THE CERN SPS

WA80 Collaboration

GSI Darmstadt
R. Albrecht, R. Bock, H.H. Gutbrod, B.W. Kolb, I. Lund, H.R. Schmidt, T. Siemiarczuk

Lawrence Berkeley Laboratory
A. Franz, P. Jacobs, A.M. Poskanzer, H.G. Ritter

Lund University
G. Claesson, A. Eklund, S. Garpman, H.Å. Gustafsson, J. Idh, P. Kristiansson, A. Oskarsson, I. Otterlund, S. Persson, E. Stenlund

Münster University
P. Beckmann, F. Berger, G. Clewing, L. Dragon, R. Glasow, K.H. Kampert, H. Löhner, M. Purschke, T. Peitzmann, R. Santo, K. Steffens, D. Stüken

Oak Ridge National Laboratory
T.C. Awes, C. Baktash, R.L. Ferguson, I.Y. Lee, F.E. Obenshain, F. Plasil, S. Saini, S.P. Sorensen, M. Tincknell, G.R. Young

VECC–BARC Calcutta
B. Sinha, Y.P. Viyogi

Spokesman: H.H. Gutbrod

225316

1. INTRODUCTION

The primary goal of WA80 is to search for the predicted quark-gluon plasma (QGP) phase transition and to study the nuclear matter at very high energy densities. A number of signatures for the QGP formation have been suggested [1, 2], and most experiments have been designed so as to obtain data that pertain to one or more of these signatures. In the case of WA80, the primary probe for the investigation of the QGP is the measurement of direct photons that may be emitted from the plasma phase. An understanding of the various predicted QGP signatures, however, requires an understanding of the background created by reaction products that do not relate directly to the QGP production and thus requires a thorough understanding of the reaction mechanisms governing nucleus-nucleus collisions at these high energies.

Consequently, another important goal of WA80 is to survey nucleus-nucleus collisions at 60 and 200 GeV/nucleon and to compare the results to those obtained from proton-nucleus interactions. We have pursued this second goal a) by measuring forward and transverse energies [3,4], b) by studying the multiplicities of produced charged particles over a large range of pseudorapidity, [5,6], c) by investigating transverse momentum spectra of neutral products [7,8], and d) by examining target fragmentation products [9].

The original experimental setup has been slightly modified for the sulfur run (fig. 1) by increasing the granularity of the multiplicity detector from approximately 30 000 pads to 45 000 pads, by installing everywhere a double layer of multiplicity detectors and changing the trigger and gating of them.

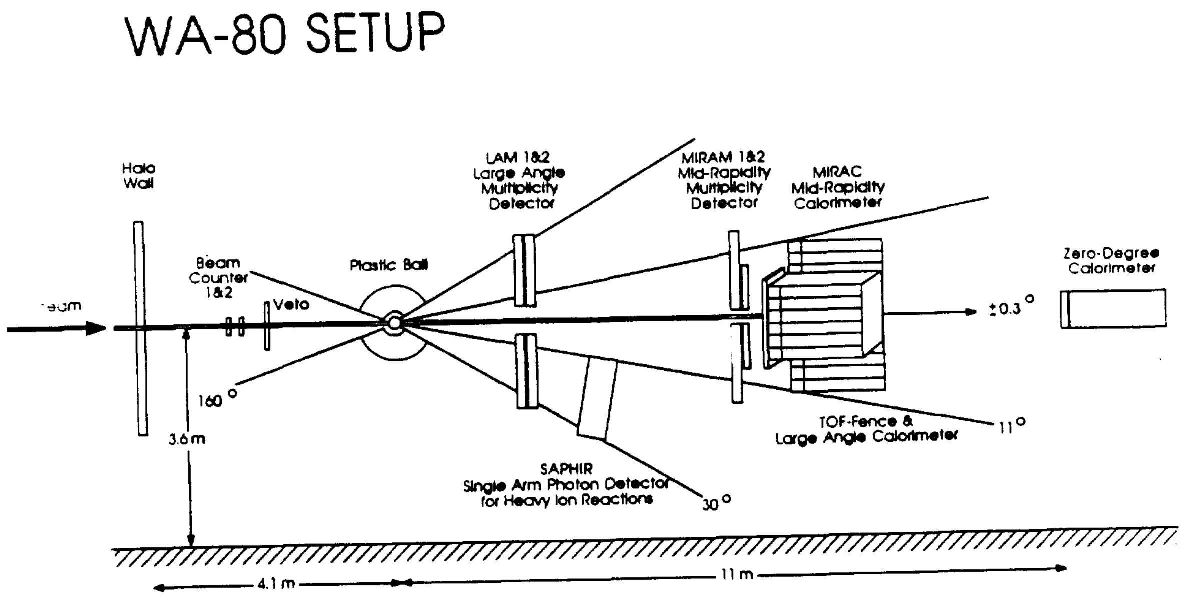

Fig. 1 : Experimental Setup of WA80 (side view)

The major point for asking more of 32 Sulfur running is coupled to the results obtained so far :

They have proven the feasability of our program especially to globally define and classify the collisions, to identify photons and reconstruct neutral pions even in the high multiplicity environment of these collisions and to extract information on single photons. While these results are very encouraging from the technical or experimental viewpoint, they have shown also interesting phenomena not explained up to now by the event generators like the LUND model in its heavy ion version (code Fritiof). These phenomena can be associated with hydrodynamical flow of the hadron phase, a necessary step in the discussion of possible phase changes.

The present results demonstrate the need for greatly increased counting statistics in order to extend the present information to much higher precision information

1. on the variation of the γ/π^0 ratio with centrality,

2. on the behavior of this ratio for P_t above 3 GeV/c, where perturbative QCD can be applied, and

3. on the behavior of this ratio for very light systems such as S + Al and p + A where little contribution from a deconfined phase is expected.

It would also be quite useful to have better information on the $\sqrt{s}$ behavior of the ratio, because the initial 'temperature' of a deconfined phase (and thus the nummer of constituent scatterings and direct photons produced) is expected to increase with $\sqrt{s}$.

In order to make this program feasable in a reasonable running time, the extension request is coupled to the following planned improvements of the experimental setup :

a. improve the experiment setup to be able to handle a beam intensity of approximately 2 x 10^6 sulfur ions per spill, close to the limit imposed by the radiation safety. This would increase the interaction rate by a factor of 2 to 2.5

b. increase the solid angle for the photon detection at least by a factor of two. This increases the number of photons measured by a factor of two, but in the reconstruction of the π^0 and the η^0 this will be a large factor, especially at low p_t.

c. increase the data taking speed by a factor of 2 to 5.

In short,
to a)
The multiplicity detectors presently are limiting the beam intensity to a level of about 800 000 sulfur ions per spill at 200 GeV/nucleon for a gold target. This is due to the current flowing in the streamer tubes. We plan to run the streamer tubes at a lower voltage which requires a more sensitive readout. Also we are looking into the possibility of devloping a new discriminator chip with many channels and having low noise and low threshold characteristics. A reduction of the current by a factor of at least 10 should give enough safety margin even for bad spill conditions.
to b)
at least 1000 more Pb-glass modules will be constructed according to the successful design of SAPHIR by the University of Muenster. More modules may be built depending on funding.
to c)
The change over from CAMAC to FASTBUS ADC's must be done now due to the add-on of 1000 more SAPHIR modules. This should yield a factor of 2.5 to 5 in speed of taking data. Together with a larger dynamic range of the ADC's the shower determination, especially of the cluster centroid, in SAPHIR will be improved.

A) Multiplicity Detector Upgrade :

The present multiplicity detector is based on a pad readout of the streamer signal with the electronics mounted directly onto the detector. After the first beamtime with heavy ions it was found that 10 % of the fired pads were due to albedo particles from the calorimeters. Due to the double layer of streamer-tubes this could be corrected in the oxygen run and was further improved for the sulfur run by increasing the granularity and shortening the gating time for the multiplicity detectors.
The results from this detection system and correlations with other components in the WA80 setup are published. Further analysis, studying for example the local and global moments of the multiplicity distribution in M, η and ϕ is presently in progress.

For the proposed upgrade, the total sum of 45 000 pads needs a small increase because of the increase in the number of SAPHIR modules. A major change in the electronics will be necessary if it is decided to run the streamer tubes at a lower voltage in order to reduce the current flowing in the streamer tubes that limits the beam intensity. The current on the wires in the streamer tubes depends on the interaction rate in the target and on the average multiplicity in the reaction, and also on the halo intensity and on the spill structure of the beam. If the current is too high it causes a voltage drop at the wire and with it a decrease in gain and, therefore, in the efficiency of the charge particle detection. This limit is reached with a beam intensity of 800 000 sulfur ions per spill on a 200mg/cm^2 gold target.

An increase in the interaction rate can only be achieved by increasing the beam intensity, since an increase in the target thickness would also increase the photon conversion probability and secondary interactions in the target.

Therefore we are considering a lowering of the operation voltage of the streamer tubes thus reducing the current and permitting an increase in the beam intensity. However, the smaller signals at the wire induce smaller signals at the pads which then requires a more sensitive discriminator than the one employed now. Fig. 2 shows the present layout per pad and the proposed change.

It is planned to develop a high density chip with more than the present 4 channels. It should allow a threshold of below 1 mV compared with the old one of 12 mV. A higher package density is also aimed at the development of a future detector with a smaller pad size for the most forward angles and very high particle densities.

This CHIP-project is discussed with Dr. P. Weilhammer from CERN, Drs. J. Alsford, L. Moult and P. Seller from Rutherford Laboratory, and will be mainly carried by GSI and University of Lund. A financial participation of CERN or the involvement of a CERN design group on the development costs (120 000.– Lbs) is requested. The costs for 5000 chips (80 000 channels) are additional 77 500 Lbs. Further costs occur for new pad boards. The LAA project has not yet a microchip, wich would meet our requirement for fast pulses.

A decision on the CHIP design and the construction is targeted for July of 1988 with a delivery date of all chips not later than July 1989. The technology of Si-pad detectors has been closely followed as an alternative for the large multiplicity detectors of WA80. Presently the granularity of the WA80 system cannot be achieved easily with silicon detectors.

B) SAPHIR upgrade

The SAPHIR detector has performed well. From the 1986 running, the data of oxygen and proton induced reactions are nearly all analyzed and parts of this analysis are already published [7,8].

Principle layout of readout electronics of one pad

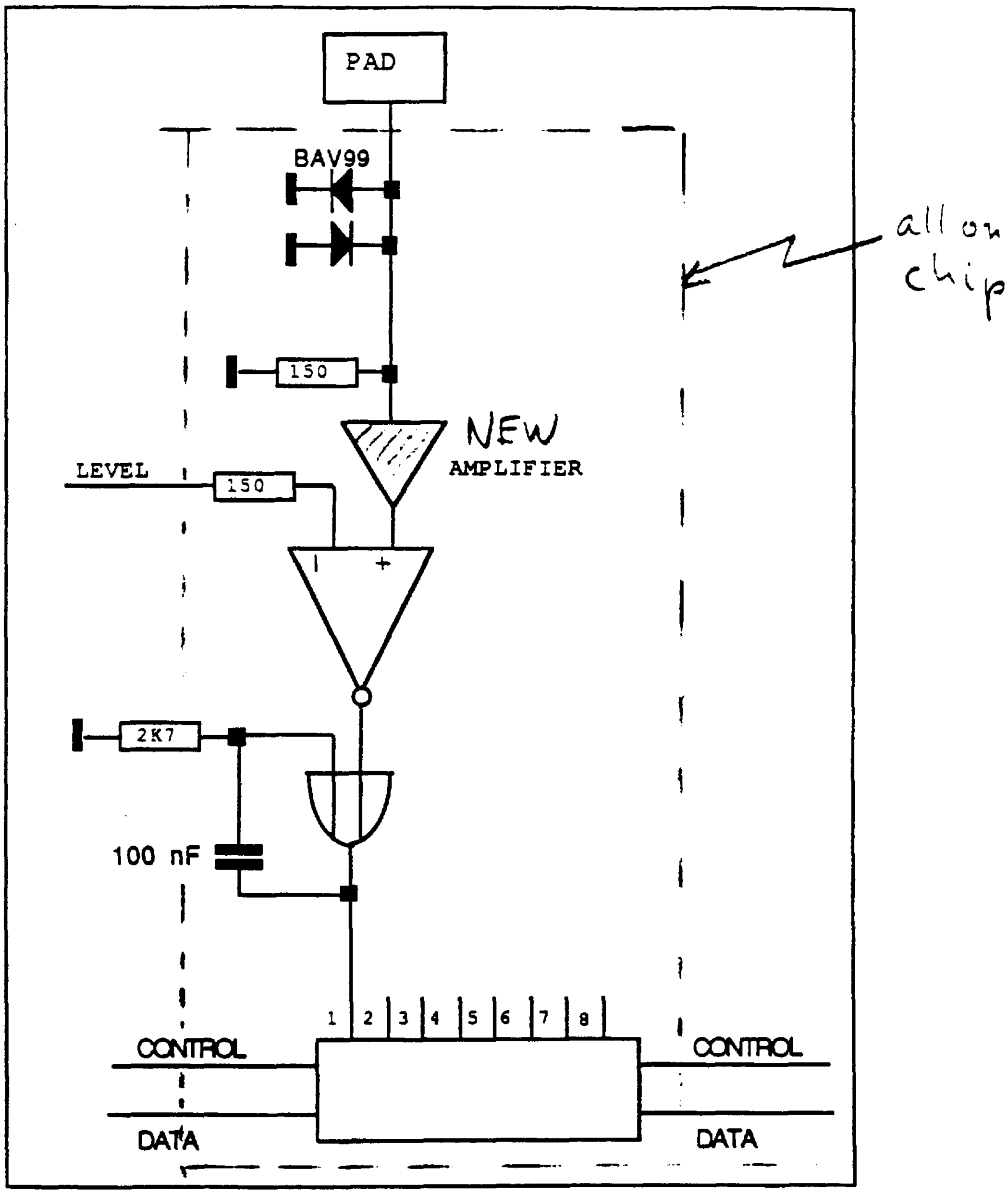

Fig. 2 : schematics of the pad electronics and the proposed change for the layout on a chip.

In short the following topics may be mentioned to describe the main results :

i. p_t spectra of inclusive photons and π^0's have been obtained and studied as a function of impact parameter and entropy density. $<p_t>$ for inclusive gammas and for π^0 change with centrality or number of participants and with the bombarding energy.

ii. η mesons have been reconstructed at $2.0 < p_t < 2.4$ GeV/c with a ratio of $\eta/\pi^0 = 74 \% \pm 23 \%$

iii. preliminary direct photon yields have been extracted for ^{16}O + Au at 200 GeV/nucleon

iv. π^0 π^0 correlations have been studied and source radii extracted for π^0 with a $p_t > 1$ GeV/c.

The analyzed data confirm the possibility to extract direct photon yields with the SAPHIR detector, but the present setup suffers from the small detection probability for η-mesons. The statistical error on the η/π − ratio contributes a large fraction to the error on the direct photon signal.
So the main effort for the upgrade will be to increase the η detection probability by increasing both the acceptance and the statistics. It is therefore planned to construct at least a second lead glass detector SAPHIR II.

The geometrical arrangement of SAPHIR I + II is sketched in fig. 3, this configuration provides the best acceptance in the same rapidity region as for SAPHIR I. The acceptances for π^0 and η^0 have been determined by Monte Carlo calculations. Fig. 4 shows the achieved improvement in η^0 − detection, especially at low p_t, as compared to the previous SAPHIR setup. This will allow to obtain $\eta^0 - p_t$ − spectra with reasonable statistical accuracy.

The reconstruction of photons in SAPHIR has proven to be very powerful even in the high multiplicity environment of Sulfur induced reactions. With the present methods of shower reconstruction the minimum distance for unambiguously separating two overlapping showers is about 5 cm. This limit can still be improved by developping a more sophisticated shower finding and fitting algorithm. This is one effort that is currently pursued to deal with the highest particle densities, i.e. very small lab-angles.

For the upgraded setup we are considering an even more flexible approach :

In addition to the mobility of the present SAPHIR in two directions we envisage to change the distance to the target. Going from 3 to 4 m would decrease the particle density by $1 - 9/16 = 44$ %. This would allow to go closer to the central rapidity region. Another important aspect is that, as the position resolution stays constant, the angular resolution and, directly connected to that, the π^0 and η mass resolution is improved at larger distances.

The incorporation of the GAMS 4000 spectrometer into the WA80 setup is still under discussion with the NA12 collaboration. This detector positioned at a distance of 6 m would offer a large variety of new possibilities following from the above considerations.

Because of compatibility and economy the design features and components of SAPHIR II will be chosen close to the SAPHIR I figures. We expect the funding for SAPHIR II to be settled during Sept. 88, and the new detector to be ready for data taking at the end of Jan. 1990. A request for funding by the German BMFT has been made by the Münster group.

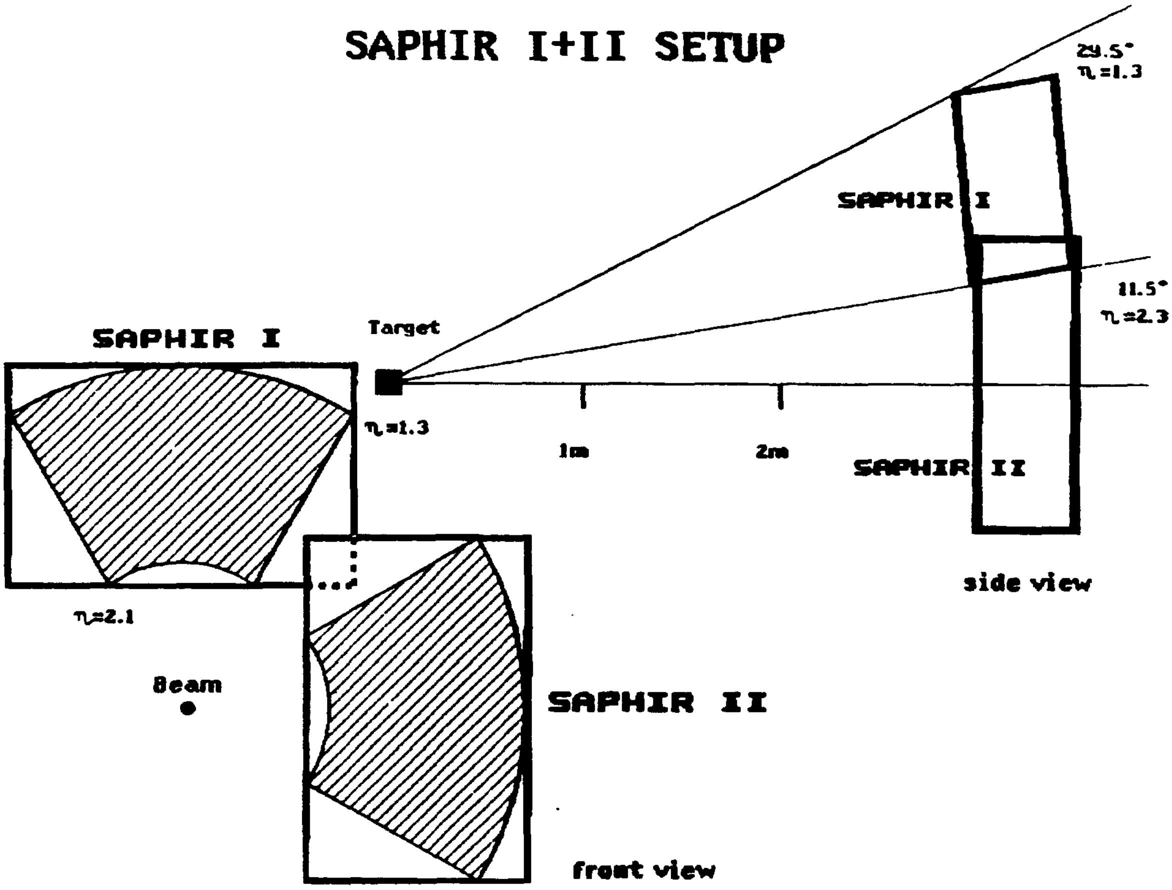

Fig. 3 : Geometrical Layout of SAPHIR I and II

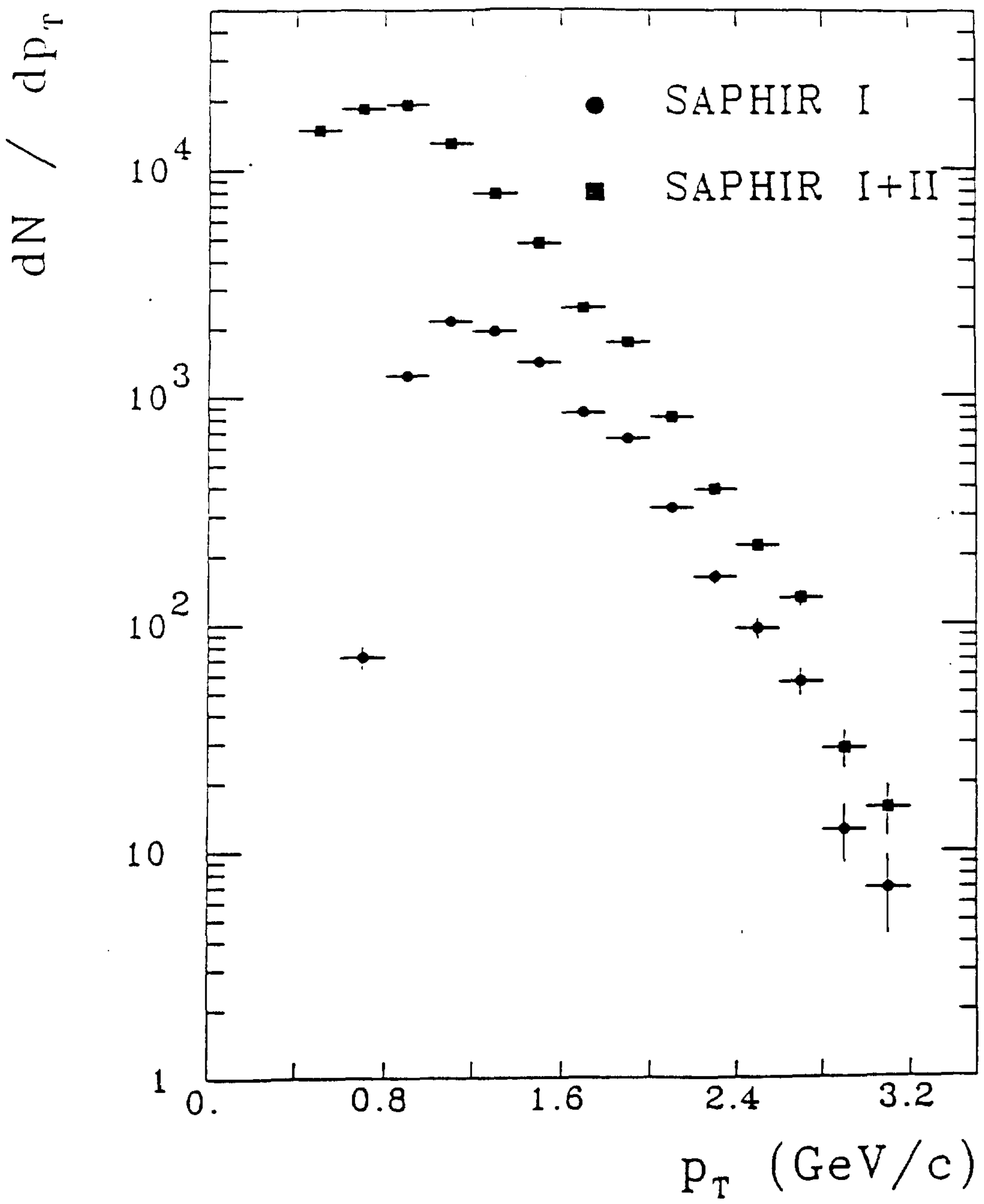

Fig. 4 : Calculations of p_t spectra of η^0 in the SAPHIR I and I + II configuration

A further source of more Pb-glass modules might be a new Indian group under the leadership of Dr. B. Sinha. They are presently producing 50 prototype modules to be tested and compared this summer with the original SAPHIR modules. This would add-if successful- another ca. 1000 to 2000 modules to our setup. The necessary photomultipliers and electronic parts would have to come from other sources. (The build up of a large quantity of SAPHIR modules is in line with the WA80 groups policy to provide a large photon detector to a Pb + Pb experiment at the future CERN-SPS lead beam.)

C) Improvements for the data acquisition of WA80

Currently, the data acquisition system of WA80 is based on CAMAC interfaced to a VAX11/750 through the micro programmable branch driver MBD. The theoretical transfer rate of the MBD is 500kbyte/s, in a realistic experiment one reaches up to 200 kbyte/s. Parallel and intelligent read-out of subsystems (REMUS, ROMULUS...) is performed through four J11 processors while the MBD transfers data of five ADC crates (2280). About 55000 channels are read out. A typical event length is 1000 to 2000 16bit words after zero supression.

Deadtime : The fixed part of the deadtime is 1.5 ms for conversion of the 2280 ADCs. Additional variable parts are ~500 x 5 μs for readout by MBD (4 ms), 500/4 x 5 μs for readout by J11s (625 μs) overlapping with conversion time of ADCs. After reset of the deadtime latch the MBD transfers data out of J11 memories (500 x 5 μs = 2.5 ms). Total deadtime is 6.5 ms (154 kword/s = 308kbyte/s).

The main bottlenecks are : The MBD transfer rate of 5 μs per word is not state of the art, the conversion time of 1.5 ms of the 2280 ADCs is too long.

Proposed changes :

We want to replace 4000 channels of LeCroy 2280 CAMAC ADCs with 5200 channels of 1882F Fastbus ADCs. The conversion time is 275 μs.

The readout proceeds via an Aleph event builder to a dual port memory which can be accessed by the VSB Interface in a VME system (VSB interface is under development at GSI). The connection of existing CAMAC modules to the VME system is done via a VSB to CAMAC interface (first modules in production at GSI). The VME system will be connected to the VAX via a VME to VAX/BI interface as developed by the CERN/DEC joint program. The eventbuilder in VME based on 68020 processor will be a CES FIC8230.

Advantages :

The faster ADCs reduce the deadtime by 1.2 ms immediately. The Fastbus ADCs have a much better resolution, the full scale range is 256 pC, thus the photomultiplier gain can be reduced. The 2280 ADCs are not any more in production and replacement parts become more expensive. The transfer rate of VME to BI interface is higher and can be used more effectively due to buffering of events in the event builder.

Expected improvement in throughput :

The CAMAC to VME transfer rate of 4Mbyte/s was tested at GSI (500 x 2 x 0.25 μs = 250 μs). The pedestal subtraction and reduction to 500 words should be performed by the Aleph event builder in Fastbus (500 μs). The Fastbus to VME transfer rate of 2Mbyte/s leads to 500 x 2 x 0.5 μs = 500 μs. This results in a total deadtime of 1250 μs compared to 4000 μs. The data rate during spills is 800kword/s. The event builder buffers the data in VME using the (spill-on)/(SPS cycle) ratio of 2.8 / 14.4 = 0.2. An average transfer rate of 311kbyte/s to VAX and tape can be achieved. This leads to an improvement factor of 800kword/s / 154kword/s = 5.2.

While the above mentioned 5200 FASTBUS ADC's are for the planned upgrade by 1000 SAPHIR modules, 4100 more FASTBUS ADC's would be required to use the GAMS 4000 detector in case it would be available to us. We are therefore requesting to CERN to provide us with 4100 channels of LeCroy FastBus ADC's during the running periods with GAMS 4000 according to the new pool policy. This would greatly reduce the disturbance to NA12 and enhance substantially their willingness to bring GAMS 4000 into WA80.

D) Triggers

Already in the oxygen and sulfur experiments we concentrated on triggers for central collisions and on the high p_t photon trigger of SAPHIR. Futhermore we concentrated on 2 targets for Oxygen : C and Au, for sulfur : Al and Au in order to get enough statistics at least for the heaviest target where plasma phenomena are to be expected and for the lightest target wich would be as close to the $p\bar{p}$ reaction as possible.
For the 60 and 120 GeV/nucleon, a trigger mix would allow to get enough data for studying the reaction mechanism but also enough photon data to obtain a good overviw.
For 200 GeV/nucleon, we will run with the photon-trigger as the main trigger selection.

E) Requests to CERN

a) Electronic Pool :

i. upgrade of pool allotment by 100 000 Sfr. for miscellaneous electronics

ii. Approximately 4100 FASTBUS ADC's (1882F from LeCroy) for the time when GAMS 4000 could be run in our experiment WA80.

b) EF-Division :

i. Financial and/or manpower participation in the chip development for a low threshold comparator

In case of a positive agreement with NA12

ii. Design and construction of a transport structure to guarantee safe transport of GAMS 4000

iii. Transport of GAMS into WA80 area.

c) From the SPS :

i. modification of the experimental area

ii. modification of the X3 beam to run low energy calibrations in our cave with good energy and position resolution.

F) Beamtime Requests

60 GeV/nucleon 32 Sulfur, (8 sec spill) 3 weeks or more

120 GeV/nucleon,(6 sec spill), 3 weeks or more

200 GeV/nucleon (4 sec spill), 10 weeks

60 and 120 GeV/c proton running with low energy extraction from the machine in order to enhance proton content in the beam.

References

[1] See, for example, Proc. Third Int. Conf. on Ultrarelativistic Nucleus-Nucleus Collisions, Brookhaven National Laboratory, Upton, N.Y., U.S.A., 1983, eds. T. Ludlam and H. Wegner, Nucl. Phys. A418 (1984); Proc. Fourth Int. Conf. on Ultrarelativistic Nucleus-Nucleus Collisions, Helsinki, Finland, 1984, ed. K. Kajantie, Lecture Notes in Physics 221 (1984) (Springer, Berlin, 1984); Proc. Fifth Int. Conf. on Ultrarelativistic Nucleus-Nucleus Collisions, Asilomar, California, U.S.A. 1986, eds. L.S. Schroeder and M. Gyulassy, Nucl. Phys. A461 (1987); L. McLerran, Rev. Mod. Phys. 58, 1021 (1986) and references therein.
[2] Van Hove, L., Nucl. Phys. A447, 443c (1985).
[3] Albrecht, R., et al., Phys. Lett. 199B, 297 (1988).
[4] Sorensen, S.P., et al., Z. Phys. C38, 3 (1988).
[4] Albrecht, R., et al., Phys. Lett. 202B 598 (1988).
[6] Lund, I., et al., Z. Phys. C38, 51 (1988).
[7] Albrecht, R., et al., Phys. Lett. 201B, 390 (1988).
[8] Loehner, H., et al., Z. Phys. C38, 97 (1988).
[9] Schmidt, H.R., et al., Z. Phys. C38, 109 (1988).
[10] Otterlund, I., et al., Quarkmatter and Astrophysics, Bombay 1988.

NORTH-HOLLAND
PHYSICS
PUBLISHING

FORWARD AND TRANSVERSE ENERGY DISTRIBUTIONS IN OXYGEN-INDUCED REACTIONS AT 60 *A* GeV AND 200 *A* GeV

WA80 Collaboration

R. ALBRECHT [a], T.C. AWES [b], C. BAKTASH [b], P. BECKMANN [c], F. BERGER [c], R. BOCK [a], G. CLAESSON [a], L. DRAGON [c], R.L. FERGUSON [b], A. FRANZ [d], S. GARPMAN [e], R. GLASOW [c], H.A. GUSTAFSSON [e], H.H. GUTBROD [a], J.W. JOHNSON [b], K.H. KAMPERT [c], B.W. KOLB [a], P. KRISTIANSSON [d], I.Y. LEE [b], H. LOHNER [c], I. LUND [a], F.E. OBENSHAIN [b,f], A. OSKARSSON [e], I. OTTERLUND [e], T. PEITZMANN [c], S. PERSSON [e], F. PLASIL [b], A.M. POSKANZER [d], M. PURSCHKE [c], H.G. RITTER [d], R. SANTO [c], H.R. SCHMIDT [a], T. SIEMIARCZUK [a,1], S.P. SORENSEN [b,f], E. STENLUND [e] and G.R. YOUNG [b]

[a] *Gesellschaft für Schwerionenforschung (GSI), D-6100 Darmstadt, Fed. Rep. Germany*
[b] *Oak Ridge National Laboratory, Oak Ridge, TN 37831, USA*
[c] *University of Munster, D-4400 Munster, Fed. Rep. Germany*
[d] *Lawrence Berkeley Laboratory, Berkeley, CA 94720, USA*
[e] *University of Lund, S-22362 Lund, Sweden*
[f] *University of Tennessee, Knoxville, TN 37996, USA*

Received 25 September 1987

Results are presented from reactions of 60 *A* GeV and 200 *A* GeV ^{16}O projectiles with C, Cu, Ag, and Au nuclei. Energy spectra measured at zero degrees and transverse energy distributions in the pseudorapidity range from 2.4 to 5.5 are shown. The average transverse energy per participant is found to be nearly independent of target mass. Estimates of nuclear stopping and of attained energy densities are made.

Reprinted from PHYSICS LETTERS B

FORWARD AND TRANSVERSE ENERGY DISTRIBUTIONS IN OXYGEN-INDUCED REACTIONS AT 60 *A* GeV AND 200 *A* GeV

WA80 Collaboration

R. ALBRECHT [a], T.C. AWES [b], C. BAKTASH [b], P. BECKMANN [c], F. BERGER [c], R. BOCK [a], G. CLAESSON [a], L. DRAGON [c], R.L. FERGUSON [b], A. FRANZ [d], S. GARPMAN [e], R. GLASOW [c], H.A. GUSTAFSSON [e], H.H. GUTBROD [a], J.W. JOHNSON [b], K.H. KAMPERT [c], B.W. KOLB [a], P. KRISTIANSSON [d], I.Y. LEE [b], H. LOHNER [c], I. LUND [a], F.E. OBENSHAIN [b,f], A. OSKARSSON [e], I. OTTERLUND [e], T. PEITZMANN [c], S. PERSSON [e], F. PLASIL [b], A.M. POSKANZER [d], M. PURSCHKE [c], H.G. RITTER [d], R. SANTO [c], H.R. SCHMIDT [a], T. SIEMIARCZUK [a,1], S.P. SORENSEN [b,f], E. STENLUND [e] and G.R. YOUNG [b]

[a] *Gesellschaft für Schwerionenforschung (GSI), D-6100 Darmstadt, Fed. Rep. Germany*
[b] *Oak Ridge National Laboratory, Oak Ridge, TN 37831, USA*
[c] *University of Munster, D-4400 Munster, Fed. Rep. Germany*
[d] *Lawrence Berkeley Laboratory, Berkeley, CA 94720, USA*
[e] *University of Lund, S-22362 Lund, Sweden*
[f] *University of Tennessee, Knoxville, TN 37996, USA*

Received 25 September 1987

Results are presented from reactions of 60 *A* GeV and 200 *A* GeV ^{16}O projectiles with C, Cu, Ag, and Au nuclei. Energy spectra measured at zero degrees and transverse energy distributions in the pseudorapidity range from 2.4 to 5.5 are shown. The average transverse energy per participant is found to be nearly independent of target mass. Estimates of nuclear stopping and of attained energy densities are made.

QCD lattice calculations [1] predict that, at sufficiently high energy densities, hadronic matter undergoes a transition to a new phase of matter, the quark–gluon plasma, in which quarks and gluons are deconfined over a relatively large volume. It has been suggested that collisions between heavy nuclei at ultrarelativistic energies may produce the energy densities, estimated to be greater than 2–3 GeV/fm^3, necessary for this phase transition to occur. An important goal of the first experiments with ultrarelativistic heavy-ion beams at the SPS accelerator at CERN is to investigate the extent to which this suggestion is correct. The primary experimental quantity used for estimating the energy density is the transverse energy, E_T [2–4]. In this paper transverse energy measurements, together with energies measured at zero degrees, are presented. It is shown that, in nucleus–nucleus collisions at ultrarelativistic energies, the transverse energy appears, to first order, to be determined by the number of participating nucleons. Estimates of nuclear stopping and of attained energy densities are also presented.

The experiment was performed with the WA80 experimental arrangement [5,6] at the CERN SPS. The setup includes two calorimeters: the Mid-Rapidity Calorimeter (MIRAC) and the Zero-Degree Calorimeter (ZDC) [7]. MIRAC consists of 30 stacks with each stack subdivided into six 20×20 cm^2 towers. Each tower consists of a lead/scintillator electromagnetic section of 15.6 radiation lengths (0.8 absorption lengths) and an iron/scintillator hadronic section of 6.1 absorption lengths. MIRAC is organized into five groups of six stacks, called six-

[1] On leave of absence from the Institute for Nuclear Studies, Warsaw, Poland.

0370-2693/87/$ 03.50 © Elsevier Science Publishers B.V. (North-Holland Physics Publishing Division)

packs, each with dimensions of 1.3×1.2 m^2. Four of the six-packs are arranged in a wall around the beam axis at a distance of 6.5 m from the target and with a 7.5×7.5 cm^2 hole in the center to allow the beam to reach the ZDC. The MIRAC wall has full azimuthal coverage in pseudorapidity, η, from 2.4 to 5.5 with partial coverage extending down to 2.0. The fifth six-pack of MIRAC is placed next to the MIRAC wall, where it covers approximately 10% of the azimuthal angles in the pseudorapidity interval from 1.6 to 2.4. The measured σ/E resolutions of the calorimeter are 14.2% for 10 GeV/c charged pions and 5.1% for 10 GeV/c electrons [7].

The ZDC is a 60×60 cm^2 uranium/scintillator calorimeter divided into an electromagnetic section of 20.5 radiation lengths and a hadronic section of 9.6 absorption lengths. The ZDC is located 11 m from the target and measures the energy of particles that pass through the beam hole in MIRAC. This hole has an inscribed cone angle of 0.3°, corresponding to $\eta > 6.0$. The ZDC is both a key component of the trigger system and an important measuring device from which the total energy of projectile spectators and/or of the leading particles is obtained. The resolution of the ZDC is 2.5% at 3.2 TeV and 4.5% at 0.96 TeV.

All data presented in this paper were obtained under the minimum bias condition. This condition is defined by the requirements that: (a) less than 88% of the full projectile energy is measured by the ZDC; and (b) at least one charged particle is recorded by the multiplicity arrays in the interval $1.3 < \eta < 4.4$. Systematic errors on the absolute cross sections are estimated to be less than 5%.

An important aspect of high energy nucleus–nucleus collisions is the nuclear collision geometry [4], as determined by the relative sizes of the target and projectile nuclei, the overlap volume in the collision, and the impact parameter. As a consequence, simple geometrical considerations can be used as a key for a qualitative understanding of the ZDC energy spectra shown in fig. 1. At 200 A GeV, the $^{16}O + ^{12}C$ reaction has essentially no cross section for events depositing a small amount energy in the ZDC because, in a simple participant spectator picture, even in the most central collisions, several projectile spectator nucleons, each with an energy of 200 GeV, proceed in the beam direction. In contrast to this, a

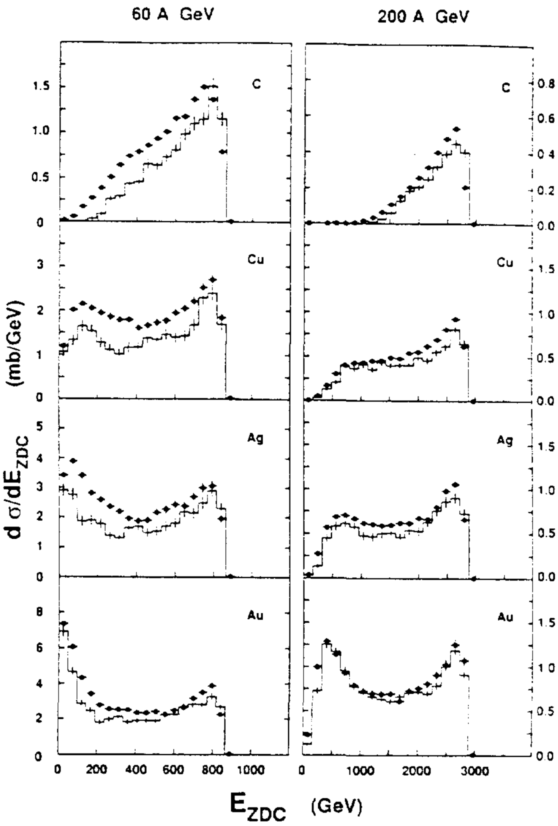

Fig. 1. Energy spectra measured in the zero-degree calorimeter (filled circles) in ^{16}O induced reactions. Histograms give the results of the FRITIOF model [8]. The vertical error bars represent statistical errors.

pronounced peak is seen at small ZDC energies in the spectrum from the $^{16}O + ^{197}Au$ reaction. In this case, events with low ZDC energies result from central collisions in which the oxygen projectile is engulfed by the massive Au nucleus, resulting in the emission of only a few leading particles at angles less than 0.3°. Furthermore, in this case, a wide range of impact parameters gives rise to collisions in which the entire projectile interacts with a nearly constant number of target nucleons, thus producing the peak at low ZDC energies.

In going from 200 A GeV to 60 A GeV the nucleon–nucleon CM rapidity decreases from 3.0 to 2.4. As a consequence, if there is no significant change in the reaction mechanism, the beam hole in MIRAC results in a more restricted ZDC coverage at the lower beam energy, and the measured integrated energy of the reaction products is correspondingly lower. This is clearly seen in the 60 A GeV $^{16}O+^{197}Au$ spectrum, which has an even more pronounced peak at the lowest energies. In the 60 A GeV $^{16}O+^{12}C$ reaction there are many more events with low ZDC energies as compared to the 200 A GeV case. These events may originate from collisions in which the oxygen projectile fragments so violently that one or more of the projectile spectators has a pseudorapidity lower than 6 and is thereby intercepted by MIRAC.

In an effort to isolate characteristic features of nucleus–nucleus collisions (e.g., collective phenomena) from those that may be expected on the basis of nucleon–nucleon or nucleon–nucleus collisions, we compare measured quantities with calculations that reproduce data from nucleon induced reactions and that make predictions from nucleus–nucleus reactions. While several models for this procedure are available, none has as yet been demonstrated to have clear advantages over the others. Consequently, we have chosen to make comparisons with the Lund model for high-energy nucleus–nucleus interactions (FRITIOF) [8]. Effects of detector acceptance and of trigger bias have been included in all FRITIOF calculations shown in this work.

The absolute cross section predictions of the FRITIOF model are shown as histograms in fig. 1. At 200 A GeV, the ZDC energy spectra are well reproduced by the calculation; whereas, at 60 A GeV, FRITIOF underestimates the cross sections, especially for the lighter targets. As discussed above, this discrepancy at 60 A GeV might be caused by projectile spectator fragmention, which is not included in the FRITIOF model. The agreement at 200 A GeV indicates that the model provides a good description of the impact-parameter dependence of the longitudinal momentum transfer.

The transverse energy produced in the reaction is measured on an event-by-event basis in MIRAC. The transverse energy is calculated as $E_T=\sum E_i \sin(\theta_i)$, where E_i and θ_i are the observed energy and the effective angle of each element i of MIRAC, respectively. The estimated systematic error in the transverse energy scale is 10%. Based on measurements of the response of the calorimeter to electrons, pions, and protons of known energies between 2 and

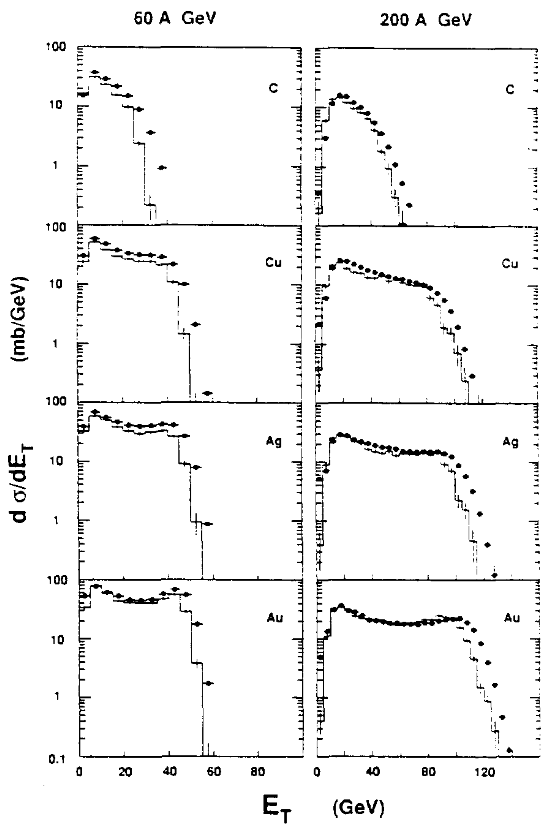

Fig. 2. Transverse energy distributions measured in the pseudorapidity range of $2.4<\eta<5.5$ for 60 A GeV and 200 A GeV ^{16}O projectiles incident on targets of C, Cu, Ag, and Au. The experimental results (filled circles) are presented with their statistical errors. Histograms give the results of the FRITIOF model.

50 GeV, an iterative procedure has been developed by means of which the nonprojective features of the calorimeter response are corrected for. The method is described in detail elsewhere [7,9].

The transverse energy distributions for $2.4<\eta<5.5$ are shown in fig. 2. As in the case of the ZDC spectra, the shapes of the E_T spectra are dominated by effects of the nuclear collision geometry. The spectra for the heaviest nuclei, Ag and Au, show a large "plateau" extending out to 80–100 GeV at 200 A GeV beam energy and to 40–45 GeV at 60 A GeV. The Au spectra have a broad peak at the high-energy end of the plateau. This peak is closely correlated with the low-energy peak in the Au ZDC spectra, as can be seen from the contour plot of $d^2\sigma/dE_T\,dE_{ZDC}$ in

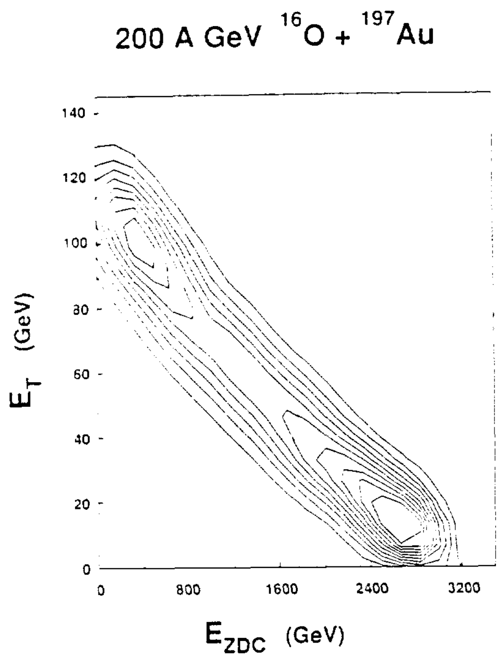

Fig. 3. Yield distributions as a function of the transverse energy (for $2.4<\eta<5.5$) and of the energy measured in the zero-degree calorimeter. The distance between the contours corresponds to a factor of two in yield.

fig. 3. This correlation demonstrates that the peak in the E_T distribution, corresponding to low ZDC energies, originates from the most central collisions, in which the entire projectile interacts with a nearly constant number of target nucleons. As the target becomes smaller, the peak and the plateau become less pronounced. For $^{16}O+^{12}C$, the E_T spectra have shapes similar to those of the E_T spectra measured in proton-induced reactions [10], whereas the heavy target spectra are similar, both in shape and energy scale, to the E_T spectra for 200 A GeV $^{16}O+Pb$ of the NA35 Collaboration [4].

At 60 A GeV, the high-energy tails of the E_T distributions for Cu, Ag, and Au targets almost coincide with one another at a value of approximately 60 GeV. This phenomenon could be caused by "complete stopping" as discussed in ref. [11]. However, at our beam energies, this finding is more likely to be due to a combination of two opposing effects. As the target mass or number of target participants increases, the maximum transverse energy increases. At the same time, however, the rapidity of the effective CM system decreases, leading to decreased coverage by MIRAC. At 60 A GeV these two effects tend to cancel each other; whereas at 200 A GeV the increase E_T dominates over the decreasing coverage, resulting in a net increase of the observed transverse energy. This demonstrates that the precise shapes of the observed E_T spectra are a sensitive function of the pseudorapidity region in which they are measured. Thus, in measurements with coverage of the lower pseudorapidity region, no peak has been seen at high E_T for heavy targets [12]. FRITIOF calculations are consistent with this observation.

The histograms in fig. 2 are the results of FRITIOF calculations. For all targets and projectile energies the model gives a good description of the shapes of the E_T spectra but consistently underestimates the transverse energy scale in the tail region by 10% to 15%.

In view of the importance of the nuclear collision geometry, it is desirable to develop a simple method by means of which the impact parameter and the number of participating nucleons can be determined. An estimate of the number of projectile participants could be obtained from the ZDC with the simple assumption that all of the observed ZDC energy is due to projectile spectators. Similarly, the number of target participants could be estimated on the assumption that all target nucleons lying in the path of the projectile are participants. This relationship between the ZDC energy and the number of projectile participants is not, however, strictly valid in the presence of leading particles or of other reaction products with $\eta>6.0$. Therefore, two alternative methods have been used to obtain a more accurate estimate of the average number of participating nucleons. First, since the ZDC data are reasonably well described by FRITIOF, the model has been used to establish a relationship between ZDC energies and the number of participants. Second, the average number of participants as a function of ZDC energy was deduced from a sharp sphere nuclear shape model together with the assumption of a monotonic increase of the impact parameter with ZDC energy and by using the relationship between impact parameter and absolute cross section. The results from both methods, shown in fig. 4 for $^{16}O+^{197}Au$

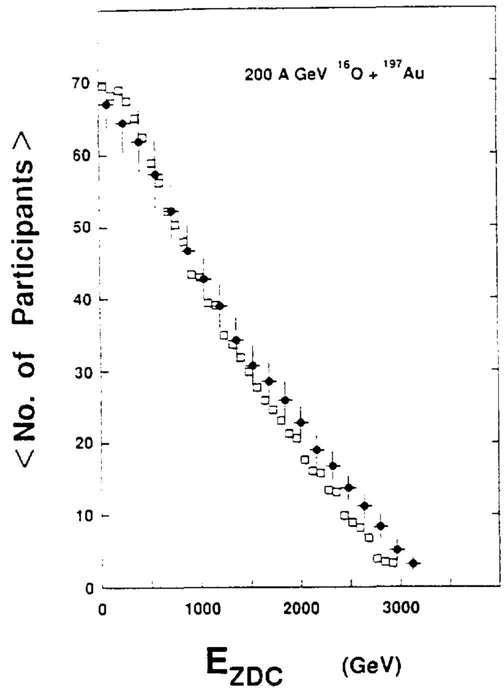

Fig. 4. The average number of participants as a function of the energy measured in the zero-degree calorimeter. The filled circles indicate the results of FRITIOF calculations, and the vertical bars indicate the standard deviations in the distributions of participants at fixed values of ZDC energy. The open squares give the results of a model independent impact parameter analysis (see text for details).

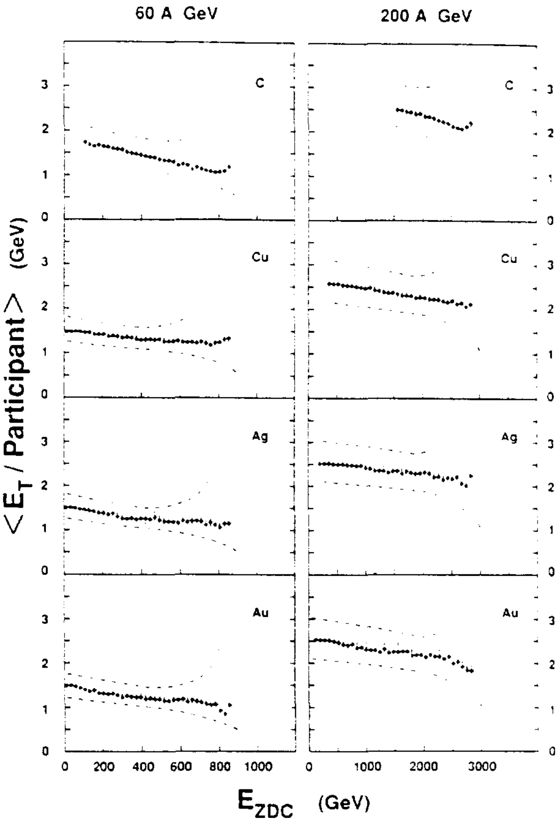

Fig. 5. Average values of E_T/participant as a function of the energy measured in the zero-degree calorimeter. The pseudorapidity range used in the E_T determination is $1.6 < \eta < 5.5$. The dashed lines indicate the estimated systematic error limits.

at 200 A GeV, are seen to be consistent with each other.

With a relationship established between the total number of participants and the ZDC energy, the E_T distributions can be examined as a function of the number of participating nucleons. In fig. 5, the average E_T per participant is shown as a function of the ZDC energy. This $\langle E_T/\text{participant}\rangle$ is calculated using the azimuthal-acceptance-corrected E_T measured in the pseudorapidity interval $1.6 < \eta < 5.5$ and the average number of participants corresponding to the observed ZDC energy. The striking feature of fig. 5 is that, at a given bombarding energy, the $\langle E_T/\text{participant}\rangle$ remains nearly constant as a function of target mass and decreases only slowly with decreasing collision centrality. Based on the above analysis, the transverse energies in central Pb+Pb collisions at 200 A GeV can be expected to be five to six times larger than those in $^{16}O+^{197}Au$ collisions. This does not, however, necessarily imply a higher energy density since the volume associated with the transverse energy production will be correspondingly larger.

The degree of nuclear stopping and the attained energy densities are two of the key quantities that relate to the probability of quark–gluon plasma formation. Estimates of these quantities based on our data are given here. Due to difficulties associated with a precise definition of "nuclear stopping", our stopping results are presented in terms of two different ratios, S_{int} and S_{mid}, between measured and theoretical values of transverse energies. The maximum value of the transverse energy, E_T^{max}, can be estimated under the assumptions that: (a) in central

Table 1
Calculation of the "integrated energy stopping" and the "mid-rapidity energy stopping" in central collisions of $^{16}O+^{197}Au$.

E_{beam}	60 A GeV	200 A GeV
N'_{part} (number of target participants)	52.0	52.0
E_{CM} (GeV)	309.2	559.1
$E'_{CM}=E_{CM}-(M^{proj}+M'_{part})c^2$ (GeV)	245.8	495.7
$E_T^{max}=\frac{1}{4}\pi E'_{CM}$ (GeV)	193.1	389.4
$[dE_T(\text{theory})/d\eta]_{max}=\frac{1}{2}E'_{CM}$ (GeV)	122.9	247.9
$E_T^{integrated}$ (GeV)	109(16)	197(30)
$[dE_T(\text{experiment})/d\eta]_{max}$ (GeV)	43(5)	66(7)
$S_{int}=E_T^{integrated}/E_T^{max}$	57(9)%	51(8)%
$S_{mid}=\dfrac{[dE_T(\text{experiment})/d\eta]_{max}}{[dE_T(\text{theory})/d\eta]_{max}}$	35(4)%	27(3)%

collisions all the projectile nucleons react with a cylinder of the target nucleus that has a base area equal to the cross section of the projectile; and (b) all of the available center-of-mass energy, E'_{CM}, is emitted isotropically in the CM system. E'_{CM} is obtained from the CM energy by subtracting the rest mass of the participating baryons. In this simple model $E_T^{max}=\frac{1}{4}\pi E'_{CM}$ and $[dE_T(\text{theory})/d\eta]_{max}=\frac{1}{2}E'_{CM}$. Numerical details of the calculation are indicated in table 1. In the analysis of the experimental data, only central events have been considered by restricting the number of participants to be larger than 24, 45, 50, and 55 for C, Cu, Ag, and Au, respectively. By fitting the experimental $dE_T/d\eta$ distribution in the interval $1.6<\eta<5.5$ with a gaussian distribution, the $E_T^{integrated}$ has been calculated as the integral of the fitted distribution. Likewise, the quantity $[dE_T(\text{experiment})/d\eta]_{max}$ has been taken to be the maximum value of the gaussian. The "integrated energy stopping", S_{int}, is defined as the ratio between $E_T^{integrated}$ and E_T^{max}. This ratio is seen from table 1 to decrease from 57% at 60 A GeV to 51% at 200 A GeV for $^{16}O+^{197}Au$. Probably a more relevant number for the stopping is the "mid-rapidity energy stopping", S_{mid}, defined as the ratio between $[dE_T(\text{experiment})/d\eta]_{max}$ and $[dE_T(\text{theory})/d\eta]_{max}$. The systematics of this quantity is shown in table 2. At 60 A GeV S_{mid} is about $\frac{1}{3}$ and only decreasing to $\frac{1}{4}$ at 200 A GeV. S_{mid} appears to be only very weakly dependent on the target mass. It should be stressed that in the above discussion of nuclear stopping the isotropic source model has only been introduced to estimate the largest possible kinematical limits.

Table 2
"Mid-rapidity energy stopping" for ^{16}O+C, Cu, Ag, and Au at 60 A GeV and 200 A GeV.

	60 A GeV	200 A GeV
C	31(3)%	21(2)%
Cu	32(3)%	26(3)%
Ag	35(4)%	26(3)%
Au	35(4)%	27(3)%

At present, no generally accepted method exists for the determination of the energy density, ε, from experimental results. We estimate ε from the following formula, which is based on the work of Bjorken [2] and which is similar to that used by Burnett et al. [3]:

$$\varepsilon=\frac{1}{\tau_0\pi R^2}\frac{dE_T}{dy}. \qquad (1)$$

Here τ_0 was taken to be 1 fm/c, and the sharp-surface electron-scattering value of 3.0 fm was used for R, the radius of ^{16}O [13]. Rapidity was replaced by pseudorapidity, and an interval of $2.4<\eta<4.0$ was used. Values of ε obtained by this prescription are believed to be underestimates of true energy densities attained [14]. Results are shown in fig. 6 for $^{16}O+^{197}Au$. The ε distribution extends to 1.3 GeV/fm^3 at 60 A GeV and as high as 2.7 GeV/fm^3 at 200 A GeV, reaching, in this case, the region of energy densities that are believed to be required for the formation of the quark–gluon plasma. The value of ε at 200 A GeV is similar to an energy density of 2.2

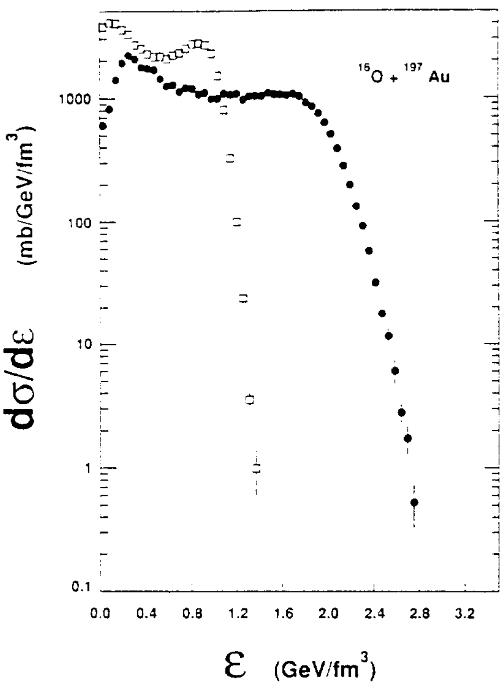

Fig. 6. Energy density distribution for 60 A GeV (open squares) and 200 A GeV (filled circles) $^{16}O+^{197}Au$ reactions as obtained from eq. (1) (see text for details concerning the calculation of ε).

GeV/fm^3 for average central collisions as measured by the NA35 Collaboration [4].

In summary, results have been presented from reactions of 60 A GeV and 200 A GeV ^{16}O projectiles with various target nuclei. Energy measurements for $\eta > 6.0$ and E_T distributions for $2.4 < \eta < 5.5$ were shown. The importance of the collision geometry was stressed. Average total participant numbers were extracted and used to show that the average transverse energy per participant is nearly independent of target mass at a given bombarding energy. Estimates of stopping and of energy densities have been made. We conclude that conditions required for the formation of the quark–gluon plasma may have been achieved in some of the most central collisions of $^{16}O+^{197}Au$ at 200 A GeV.

We appreciate the excellent work of the accelerator divisions of CERN, GSI, and LBL, which has resulted in the development and delivery of the oxygen beams used in this work. Valuable discussions with S. Pratt and C.Y. Wong are gratefully acknowledged. Partial support by the West German BMFT and DFG, the United States DOE, the Swedish NFR, the Humbolt Foundation and the CERN-EP Division is gratefully acknowledged.

References

[1] See, for example, Proc. Third Intern. Conf. on Ultrarelativistic nucleus–nucleus collisions (Brookhaven National Laboratory, Upton, NY, 1983), eds. T. Ludlam and H. Wegner, Nucl. Phys. A418 (1984);
K. Kajantie, ed. Proc. Fourth Intern. Conf. on Ultrarelativistic nucleus–nucleus collisions (Helsinki, Finland, 1984), Lecture Notes in Physics Vol. 221 (Springer, Berlin, 1984);
L.S. Schroeder and M. Gyulassy, eds., Proc. Fifth Intern. Conf. on Ultrarelativistic nucleus–nucleus collisions (Asilomar, CA, 1986), Nucl. Phys. A 461 (1987);
L. McLerran, Rev. Mod. Phys. 58 (1986) 1021, and references therein.
[2] J.D. Bjorken, Phys. Rev. D 27 (1983) 140.
[3] T.H. Burnett et al., Phys. Rev. Lett. 57 (1986) 3249.
[4] A. Bamberger et al., Phys. Lett. B 184 (1987) 271.
[5] R. Albrecht et al., Report No. GSI-85-32 (August 1985).
[6] H.H. Gutbrod et al., Proc. Intern. Workshop on Gross properties of nuclei and nuclear excitations XV (Hirschegg, Austria, 1987), ed. H. Feldmeier, Darmstadt Report ISSN 0720-8715 (1987) p. 42.
[7] T.C. Awes et al., Nucl. Instrum. Methods, to be submitted.
[8] B. Nilsson-Almqvist and E. Stenlund, Comput. Phys. Commun. 43 (1987) 387;
B. Andersson et al., Phys. Rep. 97 (1983) 31; Phys. Scr. 34 (1986) 451; Lund University Report LU-TP 86-3 (Lund, Sweden, 1986).
[9] S.P. Sorensen, Nucl. Phys. A 461 (1987) 487c.
[10] A. Franz, The transverse energy flow in hadron–lead collisions at 200 GeV/c incoming momentum, Ph. D. thesis, University of Siegen (1986);
T. Akesson et al., Nucl. Phys. A 447 (1985) 475c;
R. Gomez et al., Phys. Rev. D 35 (1987) 2736.
[11] T. Abbott et al., Phys. Lett. B 197 (1987) 285.
[12] T. Akesson et al., Z. Phys. C, to be published.
[13] H.F. Ehrenberg et al., Phys. Rev. 113 (1959) 666.
[14] L. van Hove, Proc. Second Intern. Conf. on Nucleus–nucleus collisions (Visby, Sweden, 1985), eds. H.-A. Gustafsson, B. Jakobsson, I. Otterlund, and K. Aleklett (North-Holland, Amsterdam, 1986).

PHOTON AND NEUTRAL PION DISTRIBUTIONS IN 60 AND 200 A GeV ^{16}O + NUCLEUS AND PROTON + NUCLEUS REACTIONS ☆

WA80 Collaboration

R. ALBRECHT [a], T.C. AWES [b], C. BAKTASH [b], P. BECKMANN [c], F. BERGER [c], R. BOCK [a], G. CLAESSON [a], L. DRAGON [c], R.L. FERGUSON [b], A. FRANZ [d], S. GARPMAN [e], R. GLASOW [c], H.A. GUSTAFSSON [e], H.H. GUTBROD [a], K.H. KAMPERT [c,1], B.W. KOLB [a], P. KRISTIANSSON [d], I.Y. LEE [b], H. LÖHNER [c], I. LUND [a,2], F.E. OBENSHAIN [b,f], A. OSKARSSON [e], I. OTTERLUND [e], T. PEITZMANN [c], S. PERSSON [e], F. PLASIL [b], A.M. POSKANZER [d], M. PURSCHKE [c], H.G. RITTER [d], R. SANTO [c], H.R. SCHMIDT [a], T. SIEMIARCZUK [a,3], S.P. SORENSEN [b,f], E. STENLUND [e] and G.R. YOUNG [b]

[a] *Gesellschaft für Schwerionenforschung (GSI), D-6100 Darmstadt, Fed. Rep. Germany*
[b] *Oak Ridge National Laboratory, Oak Ridge, TN 37831, USA*
[c] *University of Münster, D-4400 Münster, Fed. Rep. Germany*
[d] *Lawrence Berkeley Laboratory, Berkeley, CA 94720, USA*
[e] *University of Lund, S-22362 Lund, Sweden*
[f] *University of Tennessee, Knoxville, TN 37996, USA*

Received 2 December 1987

Transverse momentum (p_T) distributions of inclusive photons and neutral pions at midrapidity are measured with a lead glass calorimeter in 60 and 200 A GeV ^{16}O+ nucleus and proton + nucleus reactions. The variation of the average transverse momentum is investigated as function of centrality, determined by measurements of the remaining energy of the projectile and the charged particle multiplicity. For small values of the entropy, deduced from the multiplicity density, an increase in average p_T is observed levelling off for larger values of entropy. The target-mass and energy dependence of π^0 p_T distributions are presented.

Quantum chromodynamics lattice calculations [1] predict that at high nuclear density and high temperature a new phase of matter, the quark–gluon plasma (QGP) will be produced. The energy density necessary for deconfinement is estimated to be of the order of 2–3 GeV/fm^3 [2] which may be generated in heavy ion reactions at ultrarelativistic energies. First experimental results from ^{16}O + nucleus reactions [3,4] show that, in the most central events, energy densities above 2 GeV/fm^3 are reached. Since the signature of the QGP is not well established, measurements of both hadron–nucleus and nucleus–nucleus reactions have to be compared at different energies. Characteristic signals for the deconfinement phase transition [5,6] are expected from photon and lepton pair spectroscopy. Up to now, cosmic ray data have been the only source of information [7] and the observed rise of hadron transverse momenta with energy density has been interpreted as due to QGP effects [8]. In our experiment at the CERN SPS oxygen beams of 60 and 200 A GeV were used and, for comparison, p + nucleus data were taken with the same experimental setup at 60 and 200 GeV.

The details of the WA80 setup at the CERN SPS are given in ref. [9]. For the data presented in this letter the following components are of primary inter-

☆ One of us (R.S.) thanks the VW-Stiftung for the financial support during his stay at CERN in 1986.

1 Post Doctoral Fellowship from the German Research Community (DFG).

2 Post Doctoral Fellowship from Swedish Natural Research Science Council.

3 On leave of absence from the Institute of Nuclear Studies, PL-00681 Warsaw, Poland.

0370-2693/88/$ 03.50 © Elsevier Science Publishers B.V. (North-Holland Physics Publishing Division)

est: the electromagnetic lead glass calorimeter (SAPHIR), the uranium scintillator sampling calorimeter at zero degree (ZDC), and the streamer tube multiplicity arrays which cover the pseudorapidity region $1.2 \leq \eta \leq 4.2$.

The ZDC characterizes the centrality of each collision by measuring the remaining energy of projectile spectators for laboratory angles $\leq 0.3°$. A strong correlation between charged particle multiplicity and energy in ZDC is observed [10], so that both quantities may be used to distinguish between peripheral and central reactions.

SAPHIR measures the inclusive photon and π^0 distributions at midrapidity. Details of the construction and performance are given in table 1. Values for energy resolution and shower development at various angles of incidence were obtained from measurements at the DESY electron test beam (0.6–6 GeV) with a prototype detector. The complete SAPHIR setup has been tested and calibrated with electron and hadron beams (4–20 GeV) at the CERN SPS. The center of the front surface of the detector is located at 342 cm from the target and at an angle of 20° with respect to the beam direction. This gives an approximate pseudorapidity coverage of $1.5 \leq \eta \leq 2.1$ and a solid angle of 0.13 sr. Short term gain stability is continuously monitored with a nitrogen laser system. The long term stability is monitored with two independent NaI(Tl) crystals doped with Am. Light fibres conduct the laser light to the front surface of each lead glass element. The laser light intensity can be varied with filters to obtain the response of the photomultipliers over the full dynamic range and to evaluate the linearity corrections (< 5% max. deviation). The charged particle detection is achieved by two layers of plastic streamer tubes in front of the lead glass resulting in a 98% detection probability for charged particles. In order to enhance the statistics in the tail of the momentum distributions, SAPHIR is included in the trigger so that events with high energy photons are always recorded.

The streamer tube material contributes 4% to the photon conversion probability. The target vacuum chamber, a thin (500 μm) spherical aluminum chamber, contributes an additional 0.4%. Care was taken to keep all extraneous material out of the reaction zone, and background levels during target-out operation were found negligible. In addition, thin targets were used to minimize contributions from secondary interactions. The target thicknesses were 186 mg/cm^2 of C and 250 mg/cm^2 of Au, corresponding to an average photon conversion probability of 0.2% and 1.6% for C and Au, respectively. The π^0 acceptance includes the photon conversion probabilities and rises from 20% at low (0.6 GeV/c) values of the pion transverse momentum, p_T, to about 70% at 2 GeV/c and about 80% at 6 GeV/c. Error bars shown in π^0 momentum distributions include the contributions from acceptance correction uncertainties in addition to the statistical errors. The π^0 mass resolution $\sigma(M)/M$ is 5–8% (see fig. 1) and is limited mainly by variations in position resolution for different angles of incidence (non-projective geometry).

Inclusive spectra of photons, which dominantly originate from π^0 decay, have been extracted from the raw data under the following selection criteria:

(1) No hit of a charged particle is observed by the multiplicity detectors in the vicinity of a photon candidate.

(2) The transverse shower development is com-

Table 1
SAPHIR construction items and performance.

material	1278 lead glass modules SF5
module cross section	35×35 mm^2
module length	460 mm ≡ 18 radiation lengths (98% containment for 30 GeV photons)
total (rectangular) area	98×171.5 cm^2
spatial resolution	≤ 5 mm (dependent on angle of incidence)
energy resolution	$(6/\sqrt{E/\text{GeV}} + 0.4)$%
gain stability	(0.5±0.6)%
dynamic range	50 MeV – 25 GeV
minimum ionizing signal	540 MeV photon equivalent

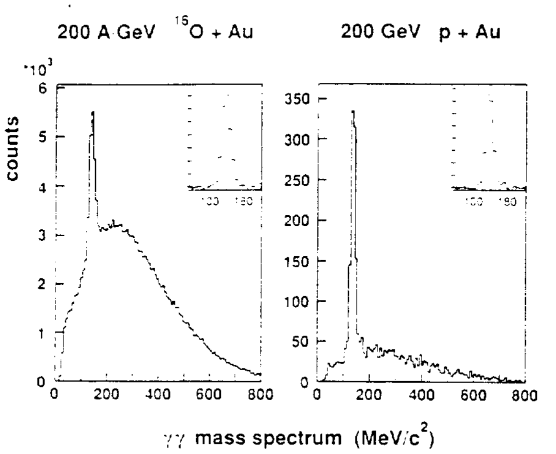

Fig. 1. Invariant mass spectra of $\gamma\gamma$ pairs for ^{16}O + Au and p + Au at 200 A GeV. Only photons with $E_\gamma > 500$ MeV and $p_{T\gamma\gamma} > 1$ GeV/c are considered. The insets show the π^0 peak after background subtraction.

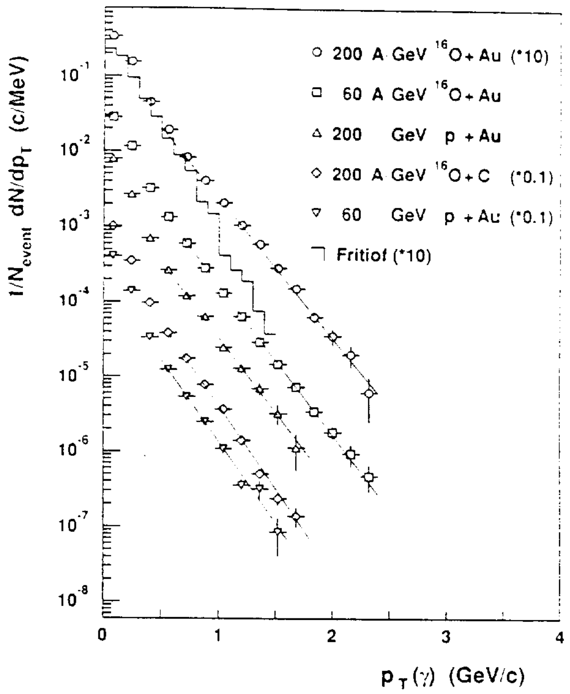

Fig. 2. Inclusive photon p_T distributions selected for central reactions with 10% of the minimum bias cross section. For comparison with exponential parametrizations (solid lines) the histogram shows the FRITIOF model results for ^{16}O + Au at 200 A GeV.

patible with that of an electromagnetic (EM) model shower of the same energy and at the same point of incidence.

The EM model showers were derived from Monte Carlo simulations, and compare reasonably well with test beam data. Since there are too few modules involved in the shower development at photon energies below 0.5 GeV, this method of EM shower selection breaks down leading to systematic errors which are included in the error bars shown in the photon spectra. For p + Au and ^{16}O + Au reactions a maximum number of 19 and 45 hits per event, respectively, were observed at 200 A GeV. From the analysis of distance distributions of hits on the SAPHIR surface we estimate an average shower overlap probability of 2%.

Fig. 2 shows inclusive photon p_T spectra containing about 10% of the minimum bias cross section after a selection of events with high charged particle multiplicity. The data are well described by an exponential parametrization $dN/dp_T \sim \exp(-p_T/T_{eff})$ for $p_T > 0.4$ GeV/c. Table 2 contains the results of a fitting procedure for the data shown in fig. 2. The slope parameters T_{eff} increase slightly with increasing target- and projectile-mass and incident energy. The experimental data are compared with the Lund model for nucleus–nucleus interactions (FRITIOF) [11]. The predicted inverse slopes are in general about 20% lower than the slope parameters fitted to the data.

We have analyzed the p_T region above 0.4 GeV/c of the inclusive photon spectra as a function of target mass and event centrality, characterized by the energy measured in the ZDC, in the following ways:

(a) fitting an exponential to the dN/dp_T distributions,

(b) calculating the average p_T from the truncated p_T distributions [12] by integrating the experimental data:

Table 2
Slope parameters T_{eff} in MeV/c from an exponential fitting procedure [$dN/dp_T \sim \exp(-p_T/T_{eff})$] for $p_T > 0.4$ GeV/c applied to the data shown in fig. 2. Errors are statistical errors only as obtained from the fit procedure.

Energy per nucleon (GeV)	p + Au	^{16}O + C	^{16}O + Au
60	198 ± 3	181 ± 2	215 ± 2
200	215 ± 4	193 ± 3	234 ± 2

$$\langle p_T \rangle_{\gamma,C} = \left(\int_C^\infty p_T \frac{dN}{dp_T} dp_T \Big/ \int_C^\infty \frac{dN}{dp_T} dp_T \right) - C, \quad (1)$$

using $C = 400$ MeV/c. Both methods give equivalent results. An example using method (b) is shown in fig. 3. Here, an increase in $\langle p_T \rangle_{\gamma,400}$ of 15% is observed for 200 A GeV ^{16}O + Au as function of the centrality as measured by the energy in the zero degree calorimeter. For the lighter systems the increase is less pronounced and lower values are observed for the lower incident energy. The FRITIOF model predicts almost no variation with centrality or target mass, however, it tends to be closer to the experiment for peripheral oxygen induced reactions and for proton induced reactions. Since the low p_T part of the spectrum tends to influence the results, the absolute numbers of $\langle p_T \rangle_{\gamma,C}$ are, of course, dependent on the choice of the cutoff value C. We find a shift in the absolute $\langle p_T \rangle_{\gamma,C}$ scale of -4% ($+4\%$) when C is changed by -80 MeV ($+120$ MeV) leaving the observed centrality dependence unchanged. Thus, the deviation from FRITIOF is obvious, although it has to be noted, that in this model hard scattering [13] is not yet included for nucleus–nucleus reactions, which may account for part of the observed effect [14].

For proton projectiles the centrality of the reaction is not well defined by the ZDC energy. In order to compare the oxygen and proton induced reactions properly and to relate the data in fig. 3 to thermodynamical models [15], we have used the entropy density [15,16] which is, except for a constant factor, given by $S = (dN/d\eta) A_{inc}^{-2/3}$. Here $dN/d\eta$ is the central multiplicity density which is approximated by the charged particle multiplicity in $1.2 < \eta < 4.2$ for different intervals in ZDC energy multiplied by 1.5 in order to correct for undetected neutral particles. A_{inc} is the mass number of the smaller colliding nucleus in central collisions. For peripheral heavy ion collisions, however, this assumption is no longer justified. Therefore A_{inc} is defined to be the number of incident projectile participants, which is derived from the ZDC energy via the FRITIOF model in close resemblance to ref. [4]. In this way the most peripheral oxygen data are expected to correspond to the proton data.

With this assumption the $\langle p_T \rangle_{\gamma,400}$ of photons as a function of the entropy density is plotted in fig. 4. We observe an increase of $\langle p_T \rangle_{\gamma,400}$ with entropy density S. Different from the proton induced reactions, the ^{16}O + Au data extend to large values of S ($S > 10$)

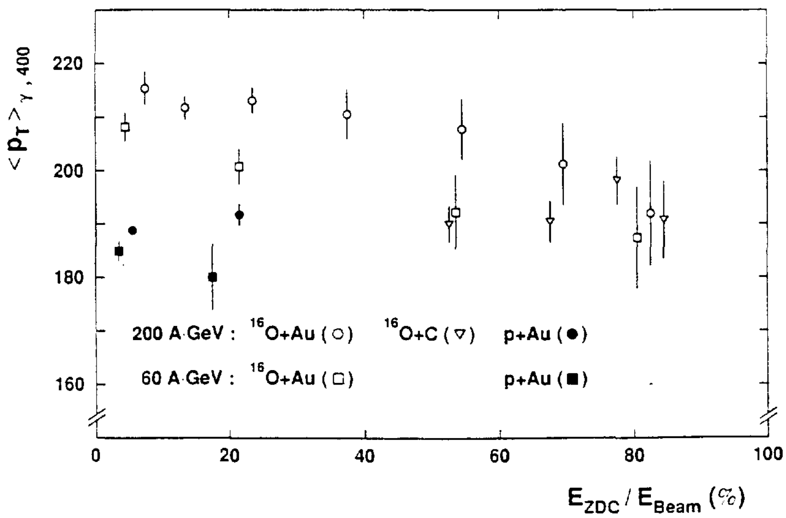

Fig. 3. Experimental $\langle p_T \rangle_{\gamma,400}$ for inclusive photons from the truncated p_T distribution (see text) as function of centrality of the reaction defined by the energy deposited in the ZDC in percent of the beam energy.

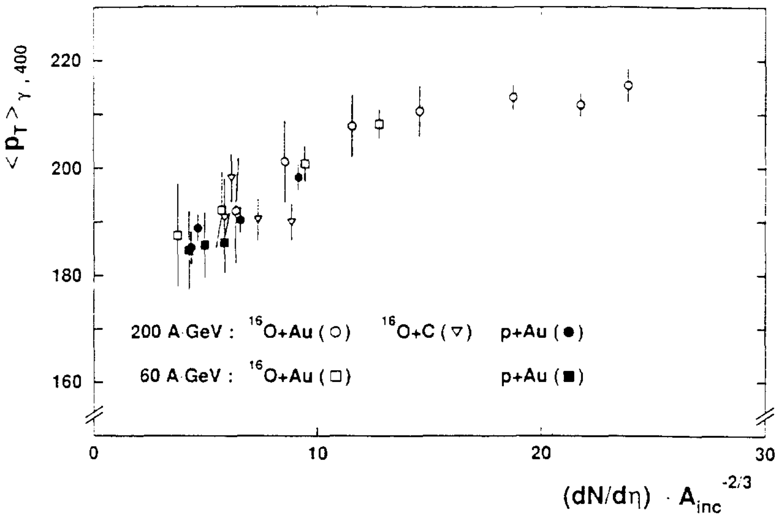

Fig. 4. Experimental $\langle p_T \rangle_{\gamma,400}$ for inclusive photons from the truncated p_T distribution (see text) as function of the entropy density estimated from the central charged particle multiplicity and the number of participating projectile nucleons which is calculated from the energy in the ZDC.

with increasing beam energy. The data points at highest S contain between 10 and 30% of the minimum bias cross section. A remarkable feature of fig. 4 is the small increase of $\langle p_T \rangle_{\gamma,400}$ at intermediate and large values of the entropy density S for ^{16}O + Au reactions at 200 A GeV. At low entropy density ($S<10$) the rise of $\langle p_T \rangle_{\gamma,400}$ may even be enhanced by up to 6% due to possible systematic errors in the photon identification. A structure like this is expected from thermodynamical and hydrodynamical studies [15,17,18] of the QGP phase transition and is reminiscent of earlier observations of cosmic ray data [7]. The relative variation of $\langle p_T \rangle_{\gamma,400}$ for p + Au at 200 GeV is consistent with data obtained from p+p and $\alpha+\alpha$ reactions at the ISR [19]. The increase to larger values of $\langle p_T \rangle$ in p+$\bar{p}$ collider data [20], where equivalently large entropy values are reached, is more closely related to the ^{16}O + Au data than to the p + Au data.

Invariant cross sections for π^0 have been obtained by analysing the invariant mass spectra of $\gamma\gamma$ pairs in small intervals of p_T. The combinatorial background below the invariant mass peak was fitted by a third order polynomial and after subtraction leads to a gaussian π^0 mass peak (fig. 1). The obtained π^0 cross sections from p + Au reactions compare within the error limits to Fermilab data [21] for π^+ and π^- from p+ W at the same incident energy and in approximately the same region of rapidity.

In fig. 5 the p_T dependence of invariant π^0 cross sections for minimum bias trigger conditions from proton and oxygen induced reactions is compared for different targets and energies. The slopes of these distributions for $p_T>0.8$ GeV/c can be described by an exponential parametrization $[(1/p_T)\, dN/dp_T \sim \exp(-p_T/T_0)]$, and slope parameters T_0 have been deduced from the same restricted transverse momentum range 0.8 GeV/$c \leqslant p_T \leqslant 2$ GeV/c for all reaction systems (table 3). The slope parameters turn out to be similar for proton and oxygen induced reactions

Table 3
Slope parameters T_0 in MeV/c for an exponential parametrization of invariant cross sections $[(1/p_T)dN/dp_T \sim \exp(-p_T/T_0)]$ for π^0 production in $1.5 \leqslant \eta \leqslant 2.1$ and for 0.8 GeV/$c \leqslant p_T \leqslant 2$ GeV/c as a function of target and projectile mass and beam energy. Errors originate from statistics and acceptance correction.

Energy per nucleon (GeV)	p + Au	^{16}O + C	^{16}O + Au
60	179 ± 13	186 ± 8	200 ± 7
200	196 ± 8	190 ± 7	210 ± 5

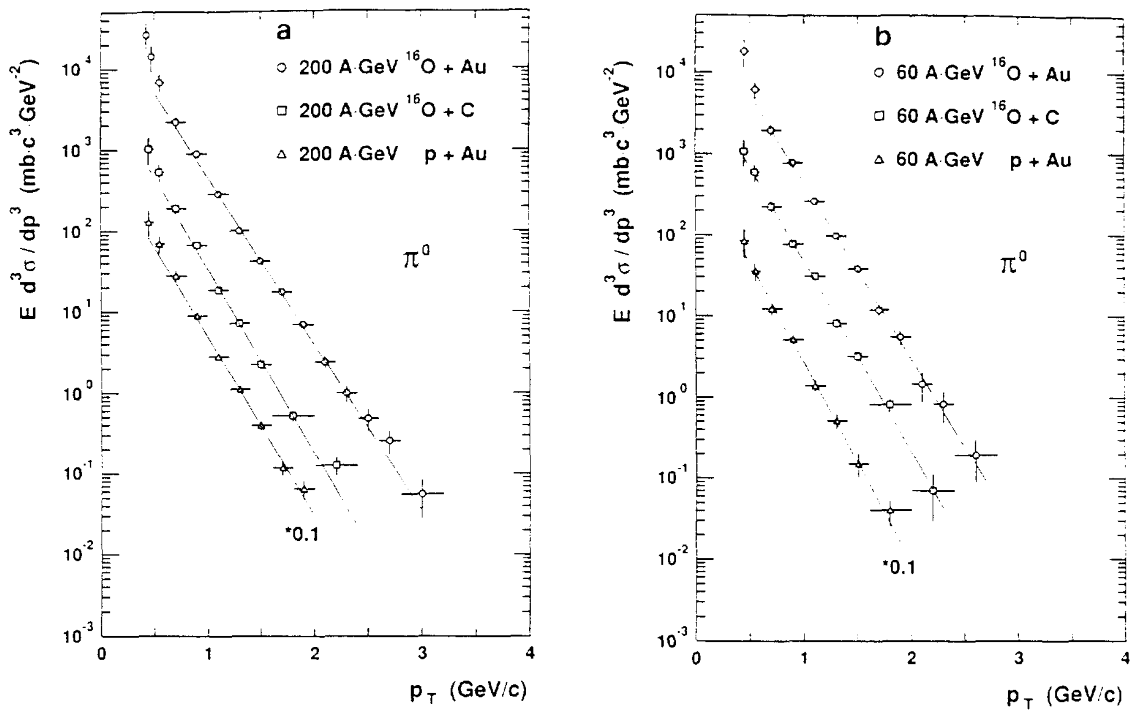

Fig. 5. Invariant cross sections for π^0 as a function of p_T from proton and oxygen induced reactions at 200 (a) and 60 A GeV (b) measured in $1.5 \leqslant \eta \leqslant 2.1$ for different target masses.

in these minimum bias data and are only weakly dependent on target mass, but are larger by at least 20% for ^{16}O + Au at 200 A GeV than for p + p reactions [22] and for FRITIOF model predictions. This behaviour is consistent with the observations cited above which show that the linear extrapolation from p + p reactions to heavy ion reactions, as contained in this model, is doubtful. In order to exclude effects from a change in the effective center-of-mass (CM) system when proton and oxygen induced reactions are compared, we investigated the η-dependence for ^{16}O + Au at 200 A GeV within the acceptance of SAPHIR ranging from 1.5 to 2.1 in η. No significant change in slope in this interval is observed which is larger than the expected change in the effective CM system.

The spectra in fig. 5 show a change in slope below $p_T \simeq 0.8$ GeV/c, which is most pronounced for the heavy system. A slope parameter $T_0 \leqslant 150$ MeV/c would be appropriate to describe the data for $p_T < 0.8$ GeV/c. This effect is not seen in 250 GeV/c p + p reactions [22], but is consistent with $\alpha+\alpha$ reactions at the ISR [12,19,23] and weakly indicated in the p+ Au data at 200 GeV. This feature is also predicted in thermodynamical models [18,24] and in studies of the hydrodynamical expansion [17,25] of the QGP.

In summary, it has been shown that even in the high multiplicity environment of ^{16}O + Au reactions the identification of π^0 in the invariant mass spectrum of $\gamma\gamma$ pairs is achieved with good accuracy in a lead glass detector. Inclusive photon spectra and p_T distributions for identified π^0 have been presented for 60 and 200 A GeV ^{16}O + nucleus and p + nucleus reactions.

The photon spectra show a target mass and centrality dependence in the region $p_T > 0.4$ GeV/c which is not predicted by the current FRITIOF model. Reactions with different initial geometry can be compared with each other when $\langle p_T \rangle$ is plotted as a function of the entropy density calculated from the multiplicty and the number of projectile participants. The levelling off of a purely linear increase of

$\langle p_T \rangle_{>400}$ with entropy density for $^{16}O + Au$ at 200 A GeV reveals features expected in the presence of a phase transition.

The π^0 p_T distributions show at least two components, a low p_T one with an inverse slope of about 150 MeV/c and a high p_T component with a flatter slope dependent slightly on target mass. These features are not compatible with a FRITIOF type linear extrapolation from p + p data to heavy ion reactions. A description in terms of a thermodynamical evolution and hydrodynamical expansion of a hot hadronic system seems to be justified and could be used for quantitative comparisons. Nevertheless, hard scattering of partons needs to be included in nucleus–nucleus scattering models, in order to study if the above observations can be explained within refined non-thermal models.

We gratefully acknowledge the support by Professor Foa (Università di Pisa), for providing us with additional lead glass modules, and by Professor Duhm, Professor Scobel, Dr. Strauss and Dr. Krause from University Hamburg during the DESY test experiments. Partial support by the West German BMFT and DFG, the United States DOE, the Swedish NFR, the Humboldt Foundation and the CERN EP-division is gratefully acknowledged.

References

[1] L. McLerran and B. Svetitsky, Phys. Lett. B 98 (1981) 195; T. Celik, J. Engels and H. Satz, Nucl. Phys. B 256 (1985) 670.

[2] M. Jacob and H. Satz, eds., Quark matter formation and heavy ion collisions, proc. Bielefeld Workshop (May 1982) (World Scientific, Singapore, 1982).

[3] A. Bamberger et al., Phys. Lett. B 184 (1987) 271.

[4] WA80 Collab., R. Albrecht et al., Phys. Lett. B 199 (1987) 297.

[5] R.C. Hwa and K. Kajantie, Phys. Rev. D 32 (1985) 1109.

[6] S. Raha and B. Sinha, Phys. Rev. Lett. 58 (1987) 101.

[7] T.H. Burnett et al., Phys. Rev. Lett. 57 (1986) 3249.

[8] E.V. Shuryak and O.V. Zhirov, Phys. Lett. B 171 (1986) 99.

[9] H.H. Gutbrod et al., GSI preprint GSI-85-32 (August 1985), CERN SPSC/85-39/M406

[10] WA80 Collab., I. Lund et al., contrib. 6 Intern. Conf. on Ultra-relativistic nucleus–nucleus collisions (Schloss Nordkirchen, 1987), Z. Phys. C, to be published.

[11] B. Nilsson-Almqvist and E. Stenlund, Comput. Phys. Commun. 43 (1987) 387.

[12] W. Bell et al., Z. Phys. C 27 (1985) 191.

[13] M. Lev and B. Petersson, Z. Phys. C 21 (1983) 155.

[14] B. Nilsson-Almqvist, contrib. High energy physics 87 Conf. (Uppsala, 1987).

[15] L. van Hove, Nucl. Phys. A 447 (1985) 443c.

[16] J.D. Bjorken, Phys. Rev. D 27 (1983) 140.

[17] M. Kataja et al., Phys. Rev. D 34 (1986) 2755.

[18] E.V. Shuryak, Phys. Rep. 61 (1980) 71.

[19] A. Breakstone et al., Phys. Lett. B 183 (1987) 227.

[20] UA1 Collab., G. Arnison et al., Phys. Lett. B 118 (1982) 167.

[21] D. Antreasyan et al., Phys. Rev. D 19 (1979) 764.

[22] NA22 Collab., P. van Hal, Thesis, CERN (1987).

[23] A.L.S. Angelis et al., Phys. Lett. B 185 (1987) 213.

[24] M. Danos and J. Rafelski, Phys. Rev. D 27 (1983) 671.

[25] J.P. Blaizot and J.Y. Ollitrault, Phys. Lett. B 191 (1987) 21.

Z. Phys. C - Particles and Fields 38, 109-115 (1988)

Zeitschrift für Physik C Particles and Fields
© Springer-Verlag 1988

Target fragmentation in proton-nucleus and ^{16}O-nucleus reactions at 60 and 200 GeV/nucleon *

H.R. Schmidt
GSI, Darmstadt, Federal Republic of Germany

WA 80 Collaboration

R. Albrecht[1], T.C. Awes[2], C. Baktash[2], P. Beckmann[3], G. Claesson[1], F. Berger[3], R. Bock[1], L. Dragon[3], R.L. Ferguson[2], A. Franz[4], S. Garpman[5], R. Glasow[3], H.Å. Gustafsson[5], H.H. Gutbrod[1], K.H. Kampert[3], B.W. Kolb[1], P. Kristiansson[4], I.Y. Lee[2], H. Löhner[3], I. Lund[1], F.E. Obenshain[2], A. Oskarsson[5], I. Otterlund[5], T. Peitzmann[3], S. Persson[5], F. Plasil[2], A.M. Poskanzer[4], M. Purschke[3], H.G. Ritter[4], R. Santo[3], H.R. Schmidt[1], T. Siemiarczuk[1], S.P. Sorensen[2], E. Stenlund[5], G.R. Young[2]

[1] Gesellschaft für Schwerionenforschung (GSI), D-6100 Darmstadt, Federal Republic of Germany
[2] Oak Ridge National Laboratory, Oak Ridge, TN 37831, USA
[3] University of Münster, D-4400 Münster, Federal Republic of Germany
[4] Lawrence Berkeley Laboratory, Berkeley, CA 94720, USA
[5] University of Lund, S-22362 Lund, Sweden

Abstract. Target remnants with $Z<3$ from proton-nucleus and ^{16}O-nucleus reactions at 60 and 200 GeV/nucleon were measured in the angular range from 30° to 160° ($-1.7<\eta<1.3$) employing the Plastic Ball detector. The excitation energy of the target spectator matter in central oxygen-induced collisions is found to be high enough to allow for complete disintegration of the target nucleus into fragments with $Z<3$. The average longitudinal momentum transfer per proton to the target in central collisions is considerably higher in the case of ^{16}O-induced reactions (≈ 300 MeV/c) than in proton-induced reactions (≈ 130 MeV/c). The baryon rapidity distributions are roughly in agreement with one-fluid hydrodynamical calculations at 60 GeV/nucleon ^{16}O+Au but are in disagreement at 200 GeV/nucleon, indicating the higher degree of transparency at the higher bombarding energy. Both, the transverse momenta of target spectators and the entropy produced in the target fragmentation region are compared to those attained in head-on collisions of two heavy nuclei at Bevalac energies. They are found to be comparable or do even exceed the values for the participant matter at beam energies of about 1-2 GeV/nucleon.

* Presented at the 6th International Conference on Ultra-Relativistic Nucleus-Nucleus Collisions - Quark Matter 1987, 24-28 August 1987, Nordkirchen, Federal Republic of Germany

I Introduction

The subject of relativistic and ultra-relativistic nuclear collisions is the study of the properties of highly excited and dense nuclear matter. The physical parameters of the fireball, formed in symmetric collisions of heavy nuclei at energies ranging from 0.1 to 2.1 GeV/nucleon have been extensively studied at the Berkeley Bevalac [10-12]. At these energies the measurement of the four-vector of most of the particles emitted from the participant fireball is experimentally possible. This goal is out of reach with present experimental techniques at ultrarelativistic energies. It is, however, possible to extend the detailed studies of participant matter at relativistic energies to "spectator" matter at ultrarelativistic energies, i.e. to investigate target fragmentation processes. Hereby it is of prime interest to investigate the mechanism and amount of momentum transfer to the target by a projectile passing through matter at practically the speed of light [7, 3]. Observables are the parallel and transverse momenta of target fragments, whose distribution should reflect the degree of transparency of nuclear matter for an ultrarelativistic projectile.

In this paper we will present first results obtained by the WA 80 collaboration with the newly available ^{16}O-ions of 60 and 200 GeV/nucleon at the

CERN SPS. Uniquely, the WA 80 experiment has the possibility to survey the target fragmentation region by its Plastic Ball [6], which covers the backward angles in the center of mass. In Sect. II we shall briefly describe the experimental setup and the data reduction. In Sect. III we shall discuss the rapidity and momentum distributions of target remnants from ^{16}O-induced reactions and compare them with those from proton-nucleus reactions. The experimental rapidity distribution will be compared with a prediction from the hydrodynamical model. In Sects. IV and V we shall extract the transverse energy and the entropy, respectively, produced in the target rapidity. The findings will be related to results from relativistic nucleus-nucleus collisions performed at the Berkeley Bevalac. Section VI will contain the investigation of collective flow effects and Sect. VII is a summary.

II Setup and data reduction

The present data were measured employing the Plastic Ball detector [6]. It, formerly used at the Berkely Bevalac as a 4π-device, is now incorporated into the WA 80-experiment [18], where it serves to measure charged particles emitted in the angular range from 30° to 160° ($-1.7<\eta<1.3$). In its present configuration, it consists of 655 $\Delta E-E$ modules arranged in a sphere. The modules are capable to identify charged π's, protons, deuterons, tritons and ^{3,4}He. At energies above 400 MeV protons can not be separated from charged pions. This uncertainty is taken account as systematic error. The data presented in this paper are characterized by the remaining energy of the projectile at small angles ($\pm 0.3°$), as measured in the zero degree calorimeter (ZDC) [2] of the WA 80-experiment. "Minimum bias" events are defined by the condition that the ZDC measures less than 90% of the full beam energy [1]. The subclass of events with low energy at $\pm 0.3°$ (< 20% at 200 GeV/nucleon) are assumed to be "central collisions".

The data are corrected for multiple hits. For the most forward positioned modules and for central collisions (high multiplicity) of ^{16}O + Au this correction amounts up to 40%. The correction integrated over the whole Ball is about 18% for central collisions and about 10% for the average "minimum bias" event. The corrections are negligible in the case of ^{16}O + Cu and C.

III Baryon distributions

Throughout the paper we will refer to the "primary reaction zone", "participating baryons" and "spectators" having the simple picture of a clean cut geometry as a working hypothesis in mind. In this geometry

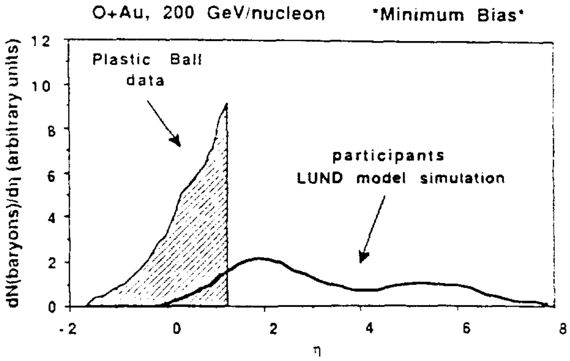

Fig. 1. Pseudorapidity distributions of target and projectile baryons. The shaded area represents the baryon distribution measured with the Plastic Ball. The solid curve is the result of a LUND model calculation yielding the participating target and projectile baryons

the primary reaction zone is a cylinder with the length of the diameter of the target nucleus and with the base equal to the cross section of the projectile nucleus. The participating baryons are contained in this cylinder and the surrounding matter is called spectator matter. To estimate the distributions of baryons steming from the primary reaction zone, the participating baryons, we have performed LUND model calculations employing the code FRITIOF [16].

Figure 1 shows the distribution of target and projectile baryons under minimum bias conditions for the reaction O + Au at 200 GeV/nucleon. The shaded area represents the baryon distribution measured with the Plastic Ball. The lower curve is the result of the model calculation. Two "bumps" at $\eta \approx 1.9$ and $\eta \approx 5.3$ are clearly seen, corresponding to the target and the projectile participants, respectively. The integrated yield of the participating baryons (from the LUND model) for an average central collisions is 75, 55, 45 and 24 baryons for the reactions O + Au, Ag, Cu and C, respectively, at 200 GeV/nucleon. These numbers are very close to those calculated assuming a "clean out" reaction geometry. The integral over the experimental η-distribution is shown in Fig. 2 for the reactions ^{16}O + Au, Ag, Cu and C as a function of the centrality of the collision. The error band accounts for the systematic uncertainty in proton identification at high energies. The most striking feature of this figure is the fact that for very central collisions the average number of baryons measured in the target rapidity region for all reactions amounts approximately to the total number of baryons of the colliding system if one subtracts the "participating" baryons from the primary reaction zone, as estimated by the LUND model. This means that for a central collisions enough energy is transferred from the projectile to the target matter to allow for complete disintegration

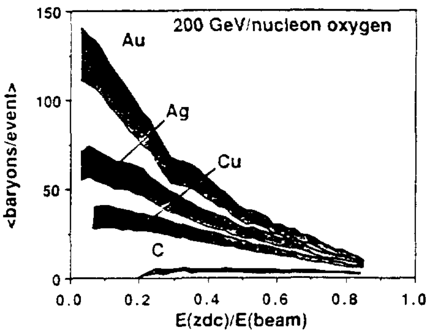

Fig. 2. Average number of baryons per event for the reaction $^{16}O + Au$ at 200 GeV nucleon as a function of the energy measured at $\pm 0.3°$ in the zero degree calorimeter. The number of baryons is corrected for multiple hits and the non-observed neutrons. The error band accounts for the systematic uncertainty in proton identification at high energies

of the target into light particles with $Z<3$. With decreasing centrality of the collisions, more and more low energy heavy fragments are produced. These particles were not detected in the Plastic Ball, resulting in the observed decrease of the average number of baryons with ZDC energy. The presence of these low energy heavy fragments, however, was clearly seen by the NA 41 experiment [5] and by Aleklett et al. [4].

III.1 Pseudorapidity distributions of baryons

Figure 3a–c shows pseudorapidity distributions of baryons from central collisions of ^{16}O on Au, Ag, Cu and C at 60 and 200 GeV/nucleon and protons on Au, Ag, Cu and C at 200 GeV. Non-observed neutrons are taken into account by weighting the proton distribution by the A/Z-ratio of the target. Since the average parallel momentum per baryon is only of the order of several hundreds of MeV/c, the pseudo-rapidity distributions are merely the angular distribution of the particles and differs drastically from the corresponding rapidity distributions (see for example Fig. 5). The distribution exhibit the following features:

i) For the reactions $^{16}O+A$ at 60 and 200 GeV/nucleon the shape of the distribution is similar for all targets and both energies while its magnitude is proportional to the target mass. The shape itself reflects the "drag" of the target baryons into the forward direction: Since the baryon distribution exhibits no distinct maximum in the η-range of the Plastic Ball a sizable fraction of the target baryons, – the participating baryons, – must appear at $\eta > 1.3$, in accordance with the above observations.

ii) For the reactions $p+A$ at 200 GeV the shape of the distribution is again similar for all targets and the magnitude is again proportional to the target mass. The shape, however, shows now a clear maximum within the Plastic Ball range at a pseudorapidity of about 0.5.

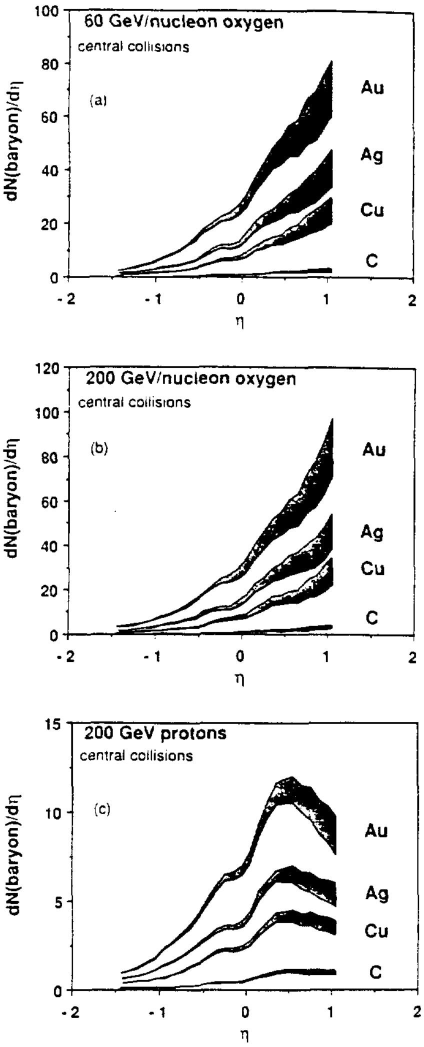

Fig. 3. a Average number of baryons per event as a function of pseudorapidity for the reaction $^{16}O + Au$, Ag, Cu and C at 60 GeV/nucleon bombarding energy. b Same as a for 200 GeV/nucleon. c Same as b for proton induced reactions

III.2 Momentum distributions of baryons

Another possibility to investigate the impact of the projectile on the target nucleus is to compare the average parallel and transverse momentum of particles for different target and projectiles. Figure 4a, b shows $\langle p_{\parallel} \rangle$/proton and $\langle p_T \rangle$/proton distributions for central collisions of 200 GeV/nucleon ^{16}O and protons on various targets. The target and projectile dependence is qualitatively the same as for the η-distributions:

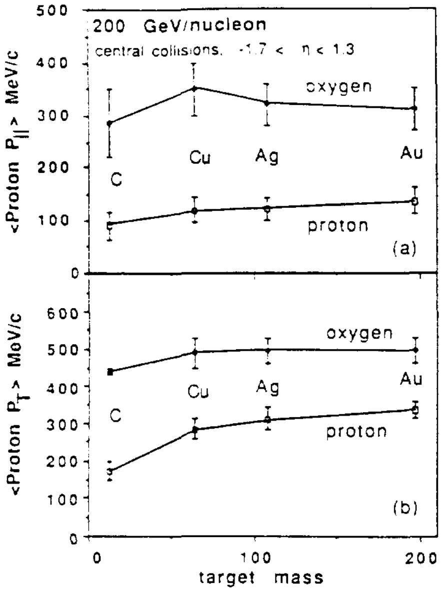

Fig. 4. a Average over the parallel momentum of protons in the pseudorapidity interval $-1.7<\eta<1.3$ as a function of the target mass. The curves through the data points are to guide the eye. The upper curve is for $^{16}O+Au$, Ag, Cu and C at 200 GeV/nucleon, the lower curve is for $p+Au$, Ag, Cu and C at 200 GeV. The error bars account for the systematic uncertainty in proton identification at high energies. b Same as a for the transverse momentum

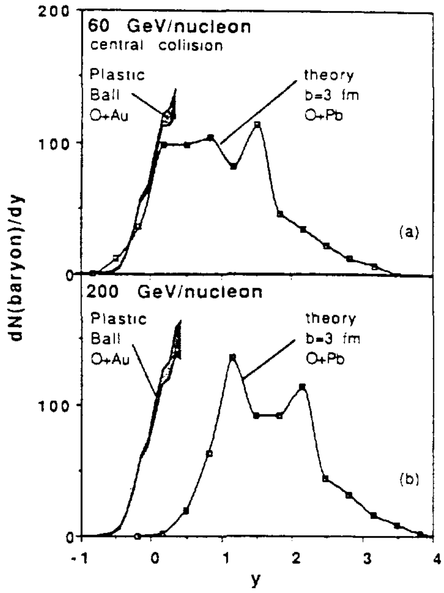

Fig. 5. a Comparison of the experimental rapidity distribution of target baryons for 60 GeV/nucleon $^{16}O+Au$ with a prediction from a one-fluid hydrodynamical model [17]. b Same as a for 200 GeV/nucleon

(i) The average momenta are fairly independent of the target nucleus.

(ii) Both the parallel and the transverse momenta of protons are significantly higher for heavy-ion induced reactions as compared to proton-nucleus reactions.

(iii) Experimentally we find no significant difference between oxygen induced reactions at 60 and 200 GeV/nucleon in the target rapidity.

The results in III.1 and III.2 demonstrate a clear difference between proton and heavy-ion induced reactions with regard to the collective acceleration of the target nucleus. They give a first clue to what happens when an ultrarelativistic heavy ion travels through target matter: A strong coupling of the projectile to the nulcear medium, which dissipates energy toward the target rapidity, seems to be of importance and modifies the simple picutre of a clean cut geometry. The similarity of ^{16}O-induced reactions at 60 and 200 GeV/nucleon shows that the acceleration of the target matter does not depend on the energy of the projectile in this energy range. It seems, however, determined by velocity of the projectile, which is practically the speed of light in both cases.

III.3 Rapidity distributions of baryons

We compare now the data with a prediction of a one-fluid hydrodynamical model [17], which represents the extreme of high stopping of the projectile in the nuclear flud. Experimental rapidity distributions of baryons, selected for central collisions, are compared with calculations performed for reactions of 200 and 60 GeV/nucleon $^{16}O+Pb$ at an impact parameter of 3 fm (Fig. 5a, b). The experimental distributions are plotted up to their apparent maximum: the distributions at larger values are strongly distorted due to the limited geometrical acceptance of the Plastic Ball. The theoretical distributions exhibit at both energies a two-component structure. The baryons at the higher rapidity might be identified as baryons coming from the primary reaction zone while particles at the lower rapidity are probably target spectators, hence those particles which are measured with the Plastic Ball detector. We find a qualitative agreement between data and theory at 60 GeV/nucleon, whereas data and the prediction disagree at 200 GeV/nucleon.

A recent analysis of the reaction $^{20}Ne+Au$ at 2.1 GeV/nucleon measured with the Plastic Ball detector at the Berkeley Bevalac [15] has shown, that for this reaction the projectile is almost fully stopped in the target nucleus. This seems to indicate, together with the above results, that the onset of nuclear transparency lies above 2.1 GeV/nucleon and close to 60 GeV/nucleon and that the degree of transparency increases from 60 GeV/nucleon to 200 GeV/nucleon.

IV Transverse energy

Transverse energies of particles emitted from a common source are a measure of the temperature of this source. Figure 6 shows the average transverse energy distribution of protons from central collisions of 200 GeV/nucleon ^{16}O on Au as a function of pseudorapidity. The width of the band represents the systematic uncertainty due to proton identification as discussed above. The transverse proton energies, taken at the maximum of the η-distribution, are plotted in Fig. 7 as a function of the centrality of the collision. Provided that this maximum can be associated with the target source, we could deduce a rapidity shift Δy of about 0.5 units for the target.

It is instructive to compare the transverse energies with those attained in collisions of equal mass heavy nuclei at Bevalac energies. In [11] average transverse energies of protons at $y_{cm}=0$ for collisions of Au + Au at bombarding energies ranging from 150 MeV/nucleon to 800 MeV/nucleon were extracted. The results are shown in Fig. 8 as a function of the reduced multiplicity. Comparing Figs. 7 and 8 we learn the surprising fact that the transverse energies of protons from ultrarelativistic collisions, emitted in the target rapidity, are considerably higher then those produced in the fireball of symmetric systems at relativistic energies. This means that target matter in ultrarelativistic heavy-ion collisions is highly excited and is comparable with participant matter created in central collisions of very heavy nuclei in the energy range of at least 1–2 GeV/nucleon.

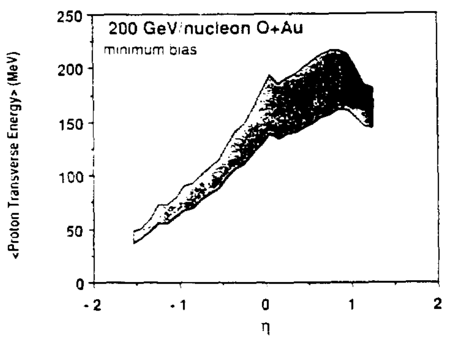

Fig. 6. Mean transverse proton energy as a function of pseudorapidity for 200 GeV/nucleon ^{16}O + Au

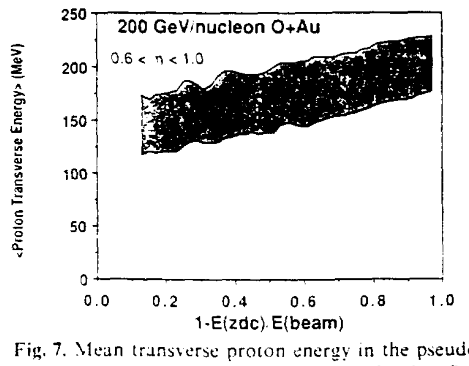

Fig. 7. Mean transverse proton energy in the pseudorapidity range $0.8 < \eta < 1.2$ as a function of centrality for 200 GeV/nucleon ^{16}O + Au

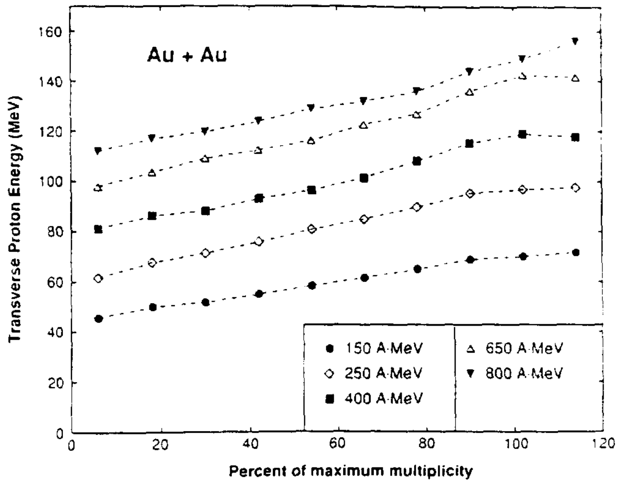

Fig. 8. Mean transverse proton energy at $y_{cm}=0$ as a function of the reduced participant proton multiplicity (N_p/N_p^{max}) for Au + Au at different beam energies between 150 and 800 MeV/nucleon

V Entropy

An observable which is assumed to carry the signature of the early stage of the collision, i.e. before the excited matter has exploded and has cooled down, is the specific entropy. If the above observation holds then the entropy of target matter should also reflect the similarity of "ultrarelativistic target matter" and "relativistic participant matter". The entropy is inferred from cluster ratio employing the Quantum Statistical Model [14] as described in Doss et al. [12]. Figure 9 shows as an example the ratio of deuteron-like to proton-like particles as a function of the centrality of the collision ^{16}O + Au at 200 GeV/nucleon. The ratios are, as described in [9], extracted only from well identified particles in a certain overlap area in phase space. As observed previously [13, 9, 12] the ratio d-like/p-like varies strongly with the impact parameter, i.e. the entropy is smallest for the most central collisions. The entropies, extracted at the maximum value of the d-like/p-like ratio, are plotted in

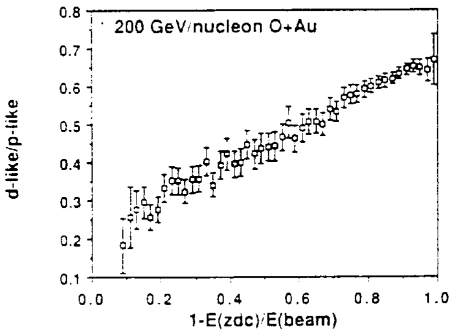

Fig. 9. Ratio of deuteron-like to proton-like particles of the reaction $^{16}O+Au$ at 200 GeV/nucleon as a function of the centrality of the reaction

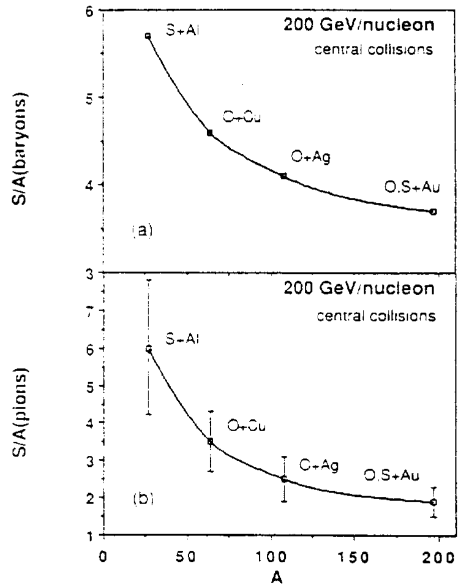

Fig. 10a, b. Dependence of the entropy per baryon for the fraction carried by baryons a and by pions b on the target mass

Fig. 10a as a function of the target mass. They show an increase of entropy as the mass of the target decreases. This decrease of entropy with target mass is similar to the decrease in entropy with the participant multiplicity [12]: in both cases the "active" volume becomes larger and hence a decreased surface to volume ratio allows for less entropy production. Again, this observation suggests a strong coupling between the projectile and the target as a whole.

Part of the entropy produced during the collision process will be carried by pionic degrees of freedom. We have roughly estimated this fraction by assuming:

(i) The non-observed neutral pions amount to half the number of the observed charged pions.

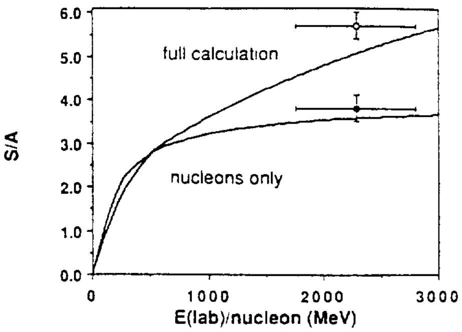

Fig. 11. Comparison of the experimental entropy per baryon produced in 200 GeV/nucleon O+Au carried by baryons only (closed squares) and by baryons and pions (open squared) with calculations. The calculations [14] are done for symmetric collisions as a function of the bombarding energy. The lower and upper curve is for the nucleonic and full (nucleonic and pionic) entropy per baryon, respectively

(ii) The entropy per pion is about four units of entropy, which is the value obtained for a massless pion gas [14].

The entropy carried by pions, normalized to the number of baryons, is shown in Fig. 10b, where we see again the decrease in entropy with increasing target mass. Differently from the case of the cluster ratios we account here for all baryons and pions falling into the acceptance window of the Plastic Ball. The error bars represent the systematic error due the lack of particle identification for very energetic protons and pions.

Like for the transverse energies it is instructive to compare the extracted entropies of "ultrarelativistic spectator matter" with the entropy of "relativistic participant matter". Figure 11 shows a calculation of the dependence of S/A on the bombarding energy for symmetric system taken from [14]. We have included the experimental entropy per baryon for the reaction $^{16}O+Au$ at 200 GeV/nucleon as the open and closed squares. Hereby the open and closed squares stand for S/A with and without the inclusion of the fraction of entropy carried by pions, respectively. The corresponding bombarding energy was determined by requiring the same ratio of the nucleonic and the full S/A for the experiment and for the calculation. As a result we obtain that the entropy of "ultrarelativistic spectator matter" is as high as the entropy of "relativistic participant matter" created in head-on collisions on heavy symmetric systems at about 2 ± 0.5 GeV/nucleon.

VI Collective flow

The Danielewicz-Odyniec transverse momentum analysis [8] has proven to be a sensitive tool to mea-

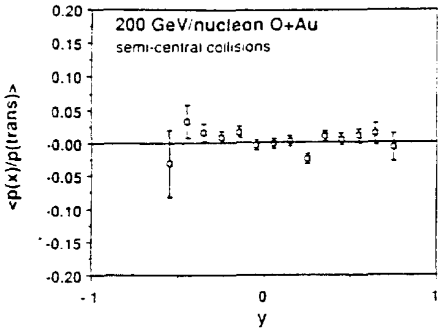

Fig. 12. Mean transverse momentum of protons projected into the reaction plane as a function of rapidity

sure collective, azimuthally asymmetric, sidewards emission of nuclear matter [10]. In order to determine the "reaction plane" of the collision from the transverse momenta the knowledge of the center of mass is essential. In our case we assume that the effective center of mass is at angles smaller than 30°, hence the reaction plane, calculated from the transverse momenta of protons in the Plastic Ball's acceptance, is determined in the backward hemisphere of the center of mass only. This assumption has been cross checked by determining the reaction plane from particles emitted at laboratory angles larger than 90° only, which yielded the same results. Figure 12 shows the result of the above discussed transverse momentum analysis for protons emitted in the reaction $^{16}O+Au$ at 200 GeV/nucleon. Here the data are selected for semi-central collisions. Differently from symmetric collisions at Bevalac energies we observe no azimuthal asymmetry of the transverse momenta distribution, indicating the absence of asymmetric sidewards flow of nuclear matter. It should be noted, however, that the method is not sensitive to an emission pattern where collective effects are azimuthally symmetric.

VII Summary and conclusion

Summarizing, we have shown that the simple picture of a clean cut geometry, involving a clear separation into "hot" participant and "cold" spectator matter has to be modified considerably: The target "spectator" matter in oxygen induced reactions at 60 and 200 GeV/nucleon is highly excited (with temperature and entropy comparable to those attained in central collisions of heavy nuclei at an energy of about 2 GeV/nucleon) and due to this high excitation energy practically no fragments heavier than $A=4$ are produced in central collisions. The rapidity of the target is probably shifted by about 0.5 units, in rough agreement with one-fluid hydrodynamical calculations [17] at 60 GeV/nucleon, but in disagreement at 200 GeV/nucleon, where the calculation predicts a too high rapidity shift of the target. From this observation we might conclude a different degree of transparency for the projectile at the two energies.

References

1. WA80-Collab. R. Albrecht et al.: Phys. Lett. B199 (1987) 297
2. T.C. Awes et al.: to be submitted to Nucl. Instrum. Methods
3. R. Anishetty, P. Koehler, L. McLerran: Phys. Rev. D (1980) 2793
4. K. Aleklett, L. Sihver, W. Loveland: Phys. Lett. B197 (1987) 34
5. B. Berthier et al.: Phys. Lett. B193 (1987) 417
6. A. Baden et al.: Nucl. Instrum. Methods 203 (1982) 189
7. H.G. Baumgardt et al.: Z. Phys. A – Atoms and Nuclei 273 (1975) 359
8. P. Danielewicz, G. Odyniec: Phys. Lett. 129B (1985) 146
9. K.G.R. Doss et al.: Phys. Rev. C32 (1985) 116
10. K.G.R. Doss et al.: Phys. Rev. C57 (1984) 302
11. K.G.R. Doss et al.: submitted to Phys. Rev. C; K.H. Kampert: Kollektive Phänomene in relativistischen Schwerionenreaktionen. Ph. D. Thesis, University of Münster (1986)
12. K.G.R. Doss et al.: accepted for publication in Phys. Rev. C
13. H.H. Gutbrod et al.: Phys. Lett. 127B (1983) 317
14. D. Hahn, H. Stöcker: LBL-22378 preprint (1986)
15. K.H. Kampert, H.R. Schmidt: private communication
16. B. Nilsson-Almqvist, E. Stenlund: Comp. Phys. Commun. 43 (1897) 387
17. T. Rentzsch et al.: Mod. Phys. Lett. A 2 (1987) 193 and private communication
18. WA80-Collab. H.R. Schmidt et al.: GSI-87-64 preprint (1987)

CHARGED-PARTICLE DISTRIBUTIONS IN ^{16}O INDUCED NUCLEAR REACTIONS AT 60 AND 200 A GeV

WA80 Collaboration

R. ALBRECHT [a], T.C. AWES [b], C. BAKTASH [b], P. BECKMANN [c], F. BERGER [c], R. BOCK [a], G. CLAESSON [a], L. DRAGON [c], R.L. FERGUSON [b], A. FRANZ [d], S.I.A. GARPMAN [e], R. GLASOW [c], H.Å. GUSTAFSSON [e,1], H.H. GUTBROD [a], J.W. JOHNSON [b], K.-H. KAMPERT [c,2], B.W. KOLB [a], P. KRISTIANSSON [d], I.Y. LEE [b], I. LUND [a,3], H. LÖHNER [c], F.E. OBENSHAIN [b], A. OSKARSSON [e], I. OTTERLUND [e], T. PEITZMANN [c], S. PERSSON [e], F. PLASIL [b], A.M. POSKANZER [d], M. PURSCHKE [c], H.G. RITTER [d], R. SANTO [c], H.R. SCHMIDT [a], T. SIEMIARCZUK [a,4], S.P. SORENSEN [b,5], E. STENLUND [e] and G.R. YOUNG [b]

[a] Gesellschaft für Schwerionenforschung (GSI), D-6100 Darmstadt, Fed. Rep. Germany
[b] Oak Ridge National Laboratory, Oak Ridge, TN 37831, USA
[c] University of Münster, D-4400 Münster, Fed. Rep. Germany
[d] Lawrence Berkeley Laboratory, Berkeley, CA 94720, USA
[e] University of Lund, Sölvegatan 14, S-22362 Lund, Sweden

Received 1 December 1987

Results from ^{16}O induced nuclear interactions with C, Cu, Ag and Au targets at 60 and 200 A GeV are presented. Multiplicity and pseudorapidity-density distributions of charged particles and their dependence on the target mass number are reported. The increase in the particle density with increasing centrality, characterized by the energy flux at zero degrees, is investigated. Comparisons with the Fritiof model reveal systematic differences.

1. Introduction

The fixed target nucleus–nucleus physics program at the CERN SPS was launched when the ^{16}O ion source [1], capable of producing highly charged ions, came into operation. The available energy scale was thereby expanded with nearly two orders of magnitude compared to Berkeley and Dubna energies. The aim of this program is to study the spacetime development of hadronic interactions under extreme conditions of energy and baryon densities within the nuclear dimensions. Central nuclear collisions are accompanied by an intense particle production [2]. In such collisons, high energy densities can be formed over large volumes, and transitions to new phases of matter, e.g. quark–gluon plasma, may occur. As a part of the WA80 [3] experimental program the multiplicity and the pseudorapidity-density distributions of charged particles are studied in 60 and 200 A GeV ^{16}O induced collisions with various nuclear targets. Characterization of an event is done via the energy flux in the forward direction, $\theta < 0.3°$, which was measured by a Zero-Degree Calorimeter (ZDC) [4] positioned 11 m downstream from the target. Essentially all the kinetic energy carried by the spectator part of the projectile is deposited in the ZDC, and consequently the energy measured there is strongly correlated to the "centrality" of the event. The data

[1] EP-Division, CERN, CH-1211 Geneva 23, Switzerland.
[2] Post Doctoral Fellowship from the German Research Community (DFG).
[3] Post Doctoral Fellowship from the Swedish Natural Science Research Council.
[4] On leave of absence from the Institute for Nuclear Studies, PL-00681 Warsaw, Poland.
[5] University of Tennessee, Knoxville, TN 37996, USA.

0370-2693/88/$ 03.50 © Elsevier Science Publishers B.V. (North-Holland Physics Publishing Division)

are compared to predictions from the event generator Fritiof [5].

2. The multiplicity detectors

A unique feature of the experiment is the large coverage in pseudorapidity, $\eta = -\ln\tan(\theta/2)$, for charged-particle detection. Between the polar angles 1.7° and 32°, η=4.2–1.2, the charged particles are measured by large multiplicity arrays consisting of Iarrocci-type streamer tubes [6]. The streamer tubes are read out through capacitively coupled pads and the position of each "fired" pad is recorded.

The first multiplicity array is placed 2.4 m from the target. In the range $10° < \theta < 32°$, $2.4 > \eta > 1.2$, it has a granular structure of 5600 pads of the sizes 5.2×3.5 and 2.1×5.2 cm^2. Further downstream, at distances of 5.8 and 6.1 m from the target, two other multiplicity arrays are placed. They both cover the angular range $1.7° < \theta < 17°$, $4.2 > \eta > 1.9$, and each of them has 8200 pads of three different sizes, 5.2×3.5, 2.1×5.2 and 1.0×2.6 cm^2, respectively. All these arrays have an area of about 9 m^2 each. A fourth, somewhat smaller array is placed below the beam axis, at a distance of 2.6 m from the target.

The Plastic Ball detector, consisting of 655 ΔE–E modules, measures all and identifies most of the charged particles in the angular range $30° < \theta < 160°$ [7]. Together, the Plastic Ball and the multiplicity detectors cover 97% of 4π sr.

The detectors are able to measure charged particles which have an energy high enough to penetrate the walls of the vacuum system, the windows of the detectors, and the air in between. For the Plastic Ball detector the thresholds are 11 MeV for protons and approximately 11 A MeV for heavier fragments. For the multiplicity arrays the thresholds are approximately 25 MeV for protons and 14 MeV for pions.

The beam particles were identified in total-reflection Čerenkov counters. Reactions in these counters were vetoed by a halo-detector. Targets of C, Cu, Ag and Au, about 200 mg/cm^2 thick, were used. Data were taken with a minimum-bias trigger which required an energy in the ZDC of less than 0.85 TeV and 2.8 TeV for 60 and 200 A GeV incident energy, respectively, and that at least one charged particle should be recorded in the multiplicity arrays. "Target-in/target-out" trigger ratios were better than 40 : 1, and the vast majority of the background events were found to have low multiplicities. To a large extent those events were rejected in the off-line analysis.

3. Corrections to the data

A charged particle traversing a streamer-tube detector produces a streamer which sometimes can be sensed by more than one pad. The "fired" pads in one detector array were therefore filtered through a cluster routine which assigns "fired" pads to clusters, hereafter called hits. Typically, 60% of the hits consist of only one "fired" pad. If more than four adjacent pads "fired", they were assigned to two or more hits.

The acceptance loss, due to the insensitivity in between the streamer tubes, sets an upper limit of the detection probability for charged particles [6]. In between the readout pads, on the circuit boards, there are also small insensitive areas. The probability of detecting a charged particle, traversing a multiplicity array, has been measured by using the information from three overlapping arrays. The overall detection probability was found to be 85%. A second method of estimating this quantity, using plastic scintillators on both sides of a detector plane for tagging, gave a similar result.

In order to separate good tracks from background tracks that do not arise from the target, hits in the different detector planes were correlated. These background tracks could for example be due to particles from secondary interactions in air and other materials, or due to albedo particles from the calorimeters in the experimental setup. In this correlation procedure the planes were used in pairs. The hits in the upstream plane were projected onto the downstream one. Candidates within a certain correlation radius, varying from 5 to 10 cm depending on the local padsizes, were considered and the one with the smallest deviation, using a cartesian norm, from the prediction in the downstream plane was used. The tracks so constructed were weighted by 0.85^{-2}. The effect of "false correlations" was studied by a Monte Carlo program. If the incoming charged particle is seen in one plane but missed in the second, a correlation could still be made with a nearby hit in that plane. These "false correlations" have been corrected for and can contribute as much as 10% to the total yield of charged particles but usually are only a few percent. In the angular region where only one detector plane was used the yield of charged particles was weighted with 0.85^{-1}. This was the reduced by a polar angle dependent factor to correct for the background tracks which do not arise from the target. This factor, typically in the order of 10–15%, was determined from the angular regions where correlations were made.

The yield of charged particles as a function of polar angle was corrected for the contributions from the following processes:

(i) γ-conversion. In order to keep the contribution from γ-conversion low, a 300–500 μm thick aluminum target-chamber and a downstream 500 μm carbon fiber beam-pipe have been employed. The correction is at most 4.4% at $\theta = 1.7°$ and goes down to 2.4% at $\theta = 8°$. Note that electron–positron pairs will almost always be assigned to the same hit.

(ii) Secondary hadronic interactions. As for γ-conversion, the probability for nuclear interactions of hadrons in the carbon-fiber beam pipe increases with decreasing polar angle. The probability is 2.6% at $\theta = 1.7°$ and decreases to 1.2% at $\theta = 8°$. Although the probabilities are quite small, the corrections are still important since each interaction can produce several charged particles, their number depending on the momentum of the incident particle. For calculating the number of charged secondaries emitted in the forward region we used a phenomenological model [8]. We estimate the total contribution from secondary hadronic interactions to be less than 7% around $\theta = 2.0°$ and then it decreases with polar angle.

(iii) Multiple-hits. The probability that two or more particles hit the same detector element depends on the particle density and the detector granularity. The highest multiple-hit probability is found in the angular region of 30–35° and for θ less than 2°. In the case of central oxygen-gold collisions at 200 A GeV these corrections are 40% and 20%, respectively. In most regions the corrections are smaller than a few percent.

γ-conversion and secondary hadronic interactions, as well as absorption, in the target are not corrected for. We estimate that for the most central collisions, where all the 16 projectile nucleons participate, the charged particle multiplicity increases due to target interactions by 1.5% on the average, the increase reaching 5% (10%) for 1% (0.1%) of these events.

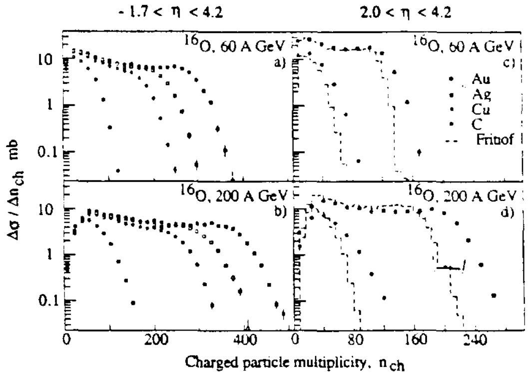

Fig. 1. Charged-particle multiplicity distributions for ^{16}O induced reactions with various targets at (a) 60 A GeV, (b) 200 A GeV, (c) 60 A GeV with $\eta > 2$, and (d) 200 A GeV, $\eta > 2$. In (c) and (d) comparisons with the Fritiof model are included.

Furthermore we have estimated the contribution to the charged-particle spectra from decaying neutral strange particles into charged decay-products. The Fritiof model predicts a relative contribution of about 7% to the total charged-particle yield from the processes $\Lambda^0 \to p\pi^-$ and $K_S^0 \to \pi^+\pi^-$. Due to the large dimensions of our experimental setup most of these decay products are observed, and consequently, they are included in the data. This fact should be kept in mind when direct comparisons with data from other experiments are made.

4. Multiplicity and pseudorapidity distributions

In figs. 1a and 1b we present the charged-particle multiplicity distributions in the range $-1.7 < \eta < 4.2$ for 60 and 200 A GeV ^{16}O interactions with C, Cu, Ag, and Au targets, samples with the minimum-bias trigger. In the very low multiplicity region a dip occurs which is dominantly a consequence of our trigger conditions. The multiplicity distribution of 200 A GeV ^{16}O+Au reactions extends to multiplicities of around 500 charged particles, which corresponds to more than 400 produced charged particles.

In order to compare with the Fritiof model [5] we exhibit in figs. 1c and 1d the multiplicity distribu-

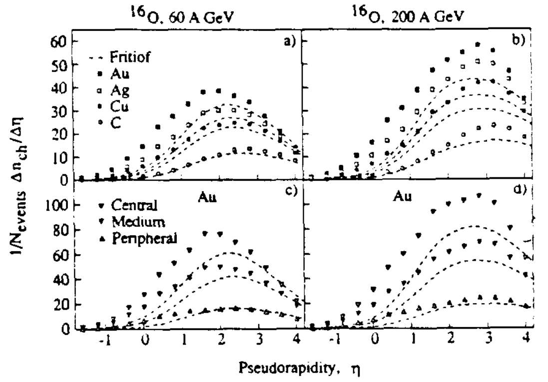

Fig. 2. Pseudorapidity-density distributions of charged particles in interactions between ^{16}O and (a) various targets at 60 A GeV, (b) various targets at 200 A GeV, (c) Au at different "centralities" at 60 A GeV, and (d) Au at different "centralities" at 200 A GeV. The statistical errors are smaller than the symbols.

tions for $2.0<\eta<4.2$. In this range the contribution from target-nucleus fragmentation, which is not included in Fritiof, is reduced. The minimum-bias trigger conditions were simulated in the model calculations. The comparison with Fritiof shows significant deviations, especially at large multiplicities, for the 200 A GeV data. These findings corroborate those of ref. [9] where also the transverse energy, E_T, is larger than the Fritiof model predictions, i.e. the excess in E_T is carried by a larger number of produced particles. (See also the inset of fig. 4).

In figs. 2a and 2b the minimum-bias pseudorapidity-density, $\rho=1/N_{events}\ (\Delta n_{ch}/\Delta\eta)$, distributions of charged particles for various targets and energies are shown. For all targets and energies the distributions are bell-shaped, and a backward shift of the maximum as the target mass increases is observed. At 60 A GeV the observed peak-shift, as a function of target mass, is about twice as large as for the 200 A GeV data. It should be pointed out that at 60 A GeV the mid-rapidity region is closer to the target fragmentation region which influences the form of the distributions. The dashed curves represent Fritiof model calculations for the different targets. Clearly, a discrepancy in the target fragmentation region is expected due to the fact that neither target fragmentation, nor intranuclear cascading are contained in the model. However, for the 200 A GeV data, a systematic deviation at mid-rapidity still remains. Presently, this deviation is not understood, and new phenomena can not be excluded. Peak-values and positions, both for the data and for the Fritiof model, are given in table 1. The shift in the peak position, as the target mass changes, is fairly well described by the Fritiof model at 200 A GeV. This shows that such shifts can be produced without involving any collectivity.

To study the deviations further, figs. 2c and 2d show the impact-parameter dependence of the charged-particle distributions in ^{16}O+Au collisions compared to the Fritiof predictions. For each energy the data have been divided into three samples, charac[illegible]ized by the energy measured by the ZDC. The se[illegible]rations were made at 90 and 270 GeV for 60 A GeV, and at 500 and 1700 GeV for 200 A GeV. Similar features as seen for the different targets are here repeated for the three different event samples. For the 200 A GeV data the relative deviations at mid-rapidity are approximately the same for the three samples.

Table 1

Features of the pseudorapidity distributions from ^{16}O induced interactions, sampled with the minimum-bias trigger, for various targets and energies. Statistical errors are ~ 1% for the peak heights (relative) and 0.1 for the peak positions (absolute).

Energy	Target	Peak height		Peak position	
		data	Fritiof	data	Fritiof
60 A GeV	Au	38.8	32.6	2.00	2.25
	Ag	30.9	27.0	2.20	2.3[illegible]
	Cu	25.3	22.9	2.36	2.[illegible]
	C	13.6	11.6	2.78	2.69
200 A GeV	Au	58.8	43.5	2.70	2.75
	Ag	51.7	36.6	2.79	2.85
	Cu	42.6	30.4	2.91	2.89
	C	23.0	16.8	3.15	3.21

5. The target mass dependence

In the inset of fig. 3 we show the target mass, A_T, dependence of the charged-particle densities, ρ, for central interactions between ^{16}O and Cu, Ag and Au at 200 A GeV. Here the centrality criterion is that less than 20% of the beam energy is deposited in the ZDC, which corresponds to events where presumably al-

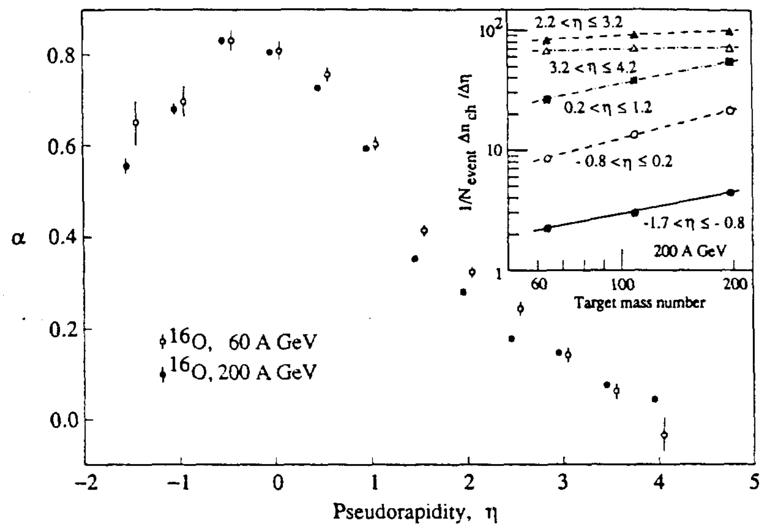

Fig. 3. The target dependence of the pseudorapidity densities, parametrized as $\rho \sim A_T^{\alpha}$, in different regions of η for ^{16}O induced interactions. The large figure shows the extracted α-values for 60 and 200 A GeV, and the inset examplifies the linear fits to obtain them. In the large figure the points for 60 A GeV are shifted 0.1 units to the right.

most all of the oxygen nucleons participate. The densities, ρ, are extracted in η-bins ranging from -1.7 to 4.2. In order to study how the charged-particle density depends on the target mass, we have chosen to use the simple parametrization $\rho \sim A_T^{\alpha}$. This parametrization gives a fairly good description of the data in all rapidity regions considered, but the exponent varies considerably with η. Fig. 3 shows $\alpha(\eta)$ as obtained by least-squares fits, examplified in the inset. The same parametrization is used for the 60 A GeV data and these results are included in fig. 3. $\alpha(\eta)$ has a maximum around $\eta=0$ and decreases rapidly with η, indicating that a "global target dependence" is strongly dependent on the rapidity region considered. α being close to one for low values of η might indicate the importance of complete target break-up. The target dependence varies smoothly over the whole η-interval and no regions where $\alpha(\eta)$ is fairly constant are observed. As η approaches 4, the projectile influence is dominant and the particle yield becomes independent of the target mass. The similarity between the two energies suggests that the target influence is essentially independent of the incident energy.

6. Transverse energy per particle

In ref. [9] the transverse energy, E_T, distributions measured by the Mid-Rapidity Calorimeter [4] were presented. The inset of fig. 4 shows the E_T versus the charged-particle multiplicity, n_{ch}, for ^{16}O + Au at 200 A GeV, both quantities measured in the η-interval 2.4 to 4.0. A linear relationship is seen. In fig. 4 we show the average E_T/n_{ch} as a function of the energy in the ZDC, at both bombarding energies and for all four targets. (Observe the broken scale on the y-axis.) It should be noted that the contribution from neutral particles is included in the E_T. The E_T/n_{ch} stays fairly constant over the total ZDC energy-range independent of projectile energy and target and has an average value of 550 MeV at both energies. An assumption of equal contributions from negative, positive, and neutral particles lowers this value to 370 MeV per particle. This is in approximate agreement with earlier findings in p–p, p–nucleus and α–α interactions [10].

7. Particle-density fluctuations and energy densities

The constant value of the average E_T/n_{ch} shows that an energy-density estimate can be made using a for-

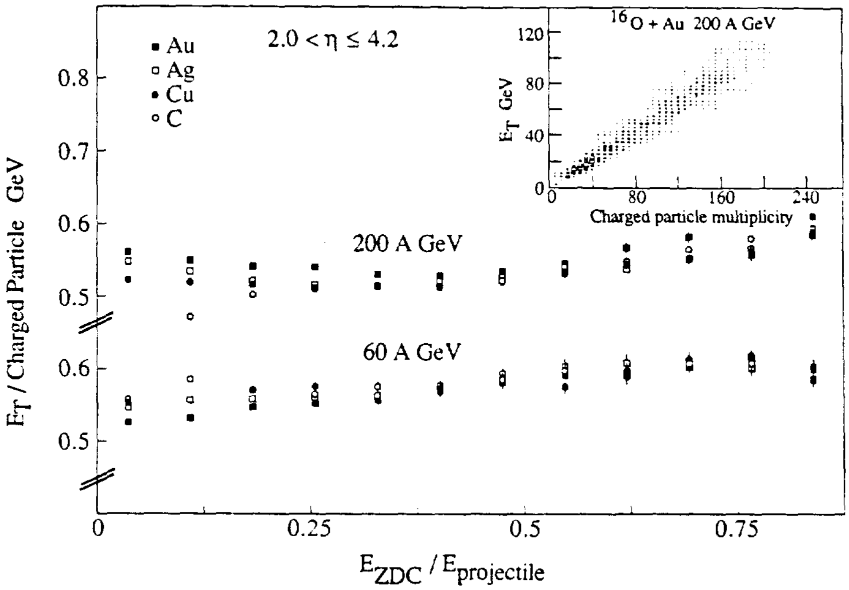

Fig. 4. E_T per charged particle for interactions between ^{16}O and various targets at 60 and 200 A GeV as a function of E_{ZDC}. The inset shows E_T versus charged-particle multiplicity for $^{16}O+Au$ reactions at 200 A GeV. Statistical errors are examplified.

mula with a constant transverse mass, e.g. $\varepsilon_0=\frac{3}{2}\rho m_T/\tau_0\pi R^2$ [11]. Here ρ is the charged-particle density, m_T is the transverse mass, τ_0 is the initial formation time, and R is the radius of the transverse reaction zone. For central collisions of oxygen on larger nuclei we have used $m_T=0.37$ GeV, $\tau_0=1$ fm/c,

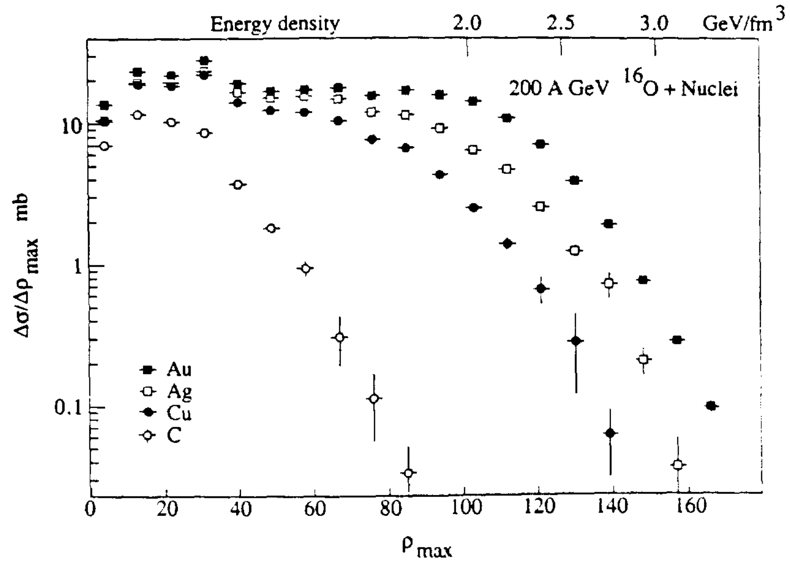

Fig. 5. Charged-particle density distributions for ^{16}O induced reactions with various targets at 200 A GeV. The upper axis shows the calculated energy density in the region of applicability [11].

$R = 1.2\,A^{1/3}$ fm, and $A = 16$. In fig. 5 we show the cross section for observing a given particle density, ρ_{max}, for the 200 A GeV data. Here ρ_{max} is defined in each event as $\Delta n_{ch}/\Delta\eta$ in the region $2.75 < \eta < 3.25$. The tails of the distributions extend to larger values of ρ_{max} as the target mass increases, and the extreme events have calculated energy densities well above 3 GeV/fm^3. This is consistent with the findings of refs. [2,9] where somewhat different methods to estimate energy densities were applied.

8. Conclusions

We have presented charged-particle distributions as a function of target mass and "centrality" of the collision. Events with more than 450 charged particles have been observed. The Fritiof model underestimates the cross section for the highest multiplicities, particularly at 200 A GeV. The pseudorapidity value where the particle density reaches its maximum is shifted backwards as the target mass increases. This behavior is in qualitative agreement with the Fritiof model. We observe an excess in the particle yield in the central rapidity region, prominent at 200 A GeV, when we compare with the model. For central collisions the target dependence of the particle yield varies strongly with the polar angle. In an A_T^{α} parametrization of the charged-particle densities, the extracted α-values range from 0.8 to 0, and a comparison with the simple geometrical expectation of $\frac{1}{3}$ is meaningful only if the full angular region is covered. Although the particle yield increases with energy, the influence of the target is almost the same at the two energies. The average transverse energy per charged particle is essentially independent of energy, target mass and "centrality" of the interaction. Particle densities up to 160 charged particles per unit pseudorapidity are readed (reached) – a value which has to await theoretical interpretations.

Acknowledgement

The authors wish to acknowledge the professional job done by the accelerator groups at CERN, GSI and LBL. We are grateful for the help obtained from the Frascati National Laboratory during the construction phase of the streamer tubes. We would like to express our deep gratitude to Pio Picchi, Per Grafström, Max Reinharz, Hubert Martine, Michel Clement and Robin Dillon for the assistance and the cooperation in the West Area, CERN. We owe a lot to Michael Marquardt, Anton Przybyla and Arno Schwinn for their devoted work with the streamer-tube detectors. Partial support by the West German BMFT and DFG, the Swedish NFR, the United States DOE, the Humboldt Foundation, and the CERN EP-division is gratefully acknowledged.

References

[1] B.H. Wolf et al., GSI-Report, GSI-86-2 (1986).
[2] A. Bamberger et al., Phys. Lett. B 184 (1987) 271.
[3] R. Albrecht et al., GSI-Report GSI-85-32 (1985).
[4] T.C. Awes et al., to be submitted to Nucl. Instrum. Methods.
[5] B. Nilsson-Almqvist and E. Stenlund, Comput. Phys. Commun. 43 (1987) 387.
[6] E. Iarrocci, Nucl. Instrum. Methods 217 (1983) 30;
G. Battistoni et al., Nucl. Instrum. Methods 217 (1983) 429;
G. Bagliesi et al., CERN-preprint, CERN-EP/87-124.
[7] A. Baden et al., Nucl. Instrum. Methods 203 (1982) 189.
[8] B. Andersson, I. Otterlund and E. Stenlund, Phys. Lett. B 84 (1979) 470.
[9] R. Albrecht et al., Phys. Lett. B 199 (1987) 297.
[10] A. Breakstone et al., Phys. Lett. B 183 (1987) 227.
[11] J.D. Bjorken, Phys. Rev. D 27 (1983) 140;
J. Cleymans, R.V. Gavai and E. Suhonen, Phys. Rep. 130 (1986) 217.